

Finger and interconnect degradations in crystalline silicon photovoltaic modules: A review

Sagarika Kumar, Roopmati Meena, Rajesh Gupta*

Department of Energy Science and Engineering, Indian Institute of Technology Bombay, Mumbai, India



ARTICLE INFO

Keywords:
 Photovoltaic module
 Defects
 Degradations
 Metallization
 Fingers
 Interconnects

ABSTRACT

The research and developments in the field of defects and degradations (D & D) in crystalline silicon photovoltaic (PV) modules have been on the forefront, to ensure reliable long term operation of solar power plants worldwide. Thereby, to maintain the overall electrical integrity and performance of cells and modules, it is essential to improve the reliability of cell metallization (i.e., busbar and fingers) and interconnects against D & D in the outdoor field conditions. This paper presents a comprehensive review and analysis on the reported D & D in conventional screen printed metallization and soldered interconnects. The review has been presented on the basis of operating modes of degradation induced via thermo-mechanical fatigue, chemical mechanisms, manufacturing fallacies, and system voltage. Furthermore, for increased understanding of the underlying defect mechanisms, these D & D have been investigated for the respective modes of electrical loss, and sensitivity to common variable parameters like position, orientation and number of defects by electrical stimulation. The use of common characterization techniques for defect detection and analysis have also been presented, wherein, the effective use of imaging techniques is advised. Also, standard environmental tests, specified under IEC 61215 were found to induce finger and interconnect D & D like in field, however, defect specific tests may be devised for a detailed analysis. Finally, the precautions performed during the manufacturing processes, especially the soldering process are identified to be key in prevention of D & D in finger and interconnects.

1. Introduction

The generation of electricity using solar photovoltaic (PV) supports the development of clean energy technologies, and also overcomes the challenges of energy security, climate change, and need of sustainable development. It is also a commercially viable technology, which offers potential for long-term growth all over the world. Currently, generation of electricity from solar PV is rapidly expanding due to the supporting policies and subsidies given by governments around the world, and also due to significant cost reductions. The PV market has experienced a compound annual growth rate of 24 % between the year 2010–2017 [1]. However, affordability, reliability, and sustainability are key pillars for operation and expansion of any energy system [2]. Even though, solar PV is gradually becoming affordable, it still needs to gain more confidence for its long term reliable operation, since it is vulnerable to defects and degradations (D & D).

The reliability of PV modules is a key aspect, which ensures its smooth operation and performance during its working condition in the outdoor field. In this direction, research conducted on reliability of

crystalline silicon (c-Si) PV modules are of paramount importance, as the technology contributes to more than 95 % of the worldwide PV production, amongst other technologies [1]. In this technology, generally the p-n junction within the cell is fabricated near to one side of wafer, and the metallic contacts are provided on both sides of the wafer, for collection and conduction of current generated in the cell. The metallic grid is provided on front side of the cell, while optimizing the shading losses and series resistance. The most conventional metallization technology used on c-Si PV cell is the screen printing technology for printing silver fingers and busbars on cell wafers [3]. It is the most widely used metallization manufacturing process due to its low cost, potential of scalability, ease of operation, and high throughput. For connection of the cells into modules, a copper ribbon is commonly soldered over the busbars to form connection between different cells. The intertwined network of fingers, busbar, and interconnects allow the collection and conduction of current, and are thereby essential in maintaining the electrical integrity of the cell and module operation. Henceforth, a defect or degradation causing anomaly with their structure, chemical composition, or design, affects the overall performance and reliability of PV cells and modules.

* Corresponding author.

E-mail address: rajeshgupta@iitb.ac.in (R. Gupta).

Abbreviations	
D & D	Defects and Degradations
PV	Photovoltaic
c-Si	Crystalline Silicon
EVA	Ethylene vinyl acetate
UV	Ultra-violet
TC	Thermal cycle
HF	Humidity freeze
DH	Damp Heat
IEC	International electro-technical commission
I-V	Current-voltage
NDT	Non-destructive testing
EL	Electroluminescence
PL	Photoluminescence
IR	Infrared
DLIT	Dark lock-in thermography
LBIC	Light beam induced current
FTIR	Fourier transform infrared
XPS	X-ray photoelectron spectroscopy
SEM	Scanning electron microscopy
EDS	Energy dispersive spectroscopy
TEM	Transmission electron microscopy
EPMA	Electron probe micro-analyzer
ToF-SIMS	Time-of-Flight Secondary Ion Mass Spectrometry
AEM	Auger Electron (Emission) Spectroscopy
IQE	Internal quantum efficiency
P _{out}	Cell or module output power
R _{series}	Series resistance
V _{oc}	Open circuit voltage
I _{sc}	Short circuit current
FF	Fill factor
CTE	Coefficient of thermal expansion
IMC	Intermetallic compound
IEA	International Energy Agency
PID	Potential induced degradation
°C	Degree Celcius
RH	Relative humidity
W	Watt
A	Current
V	Volt
m	Milli
μ	Micro
Ω	Ohms

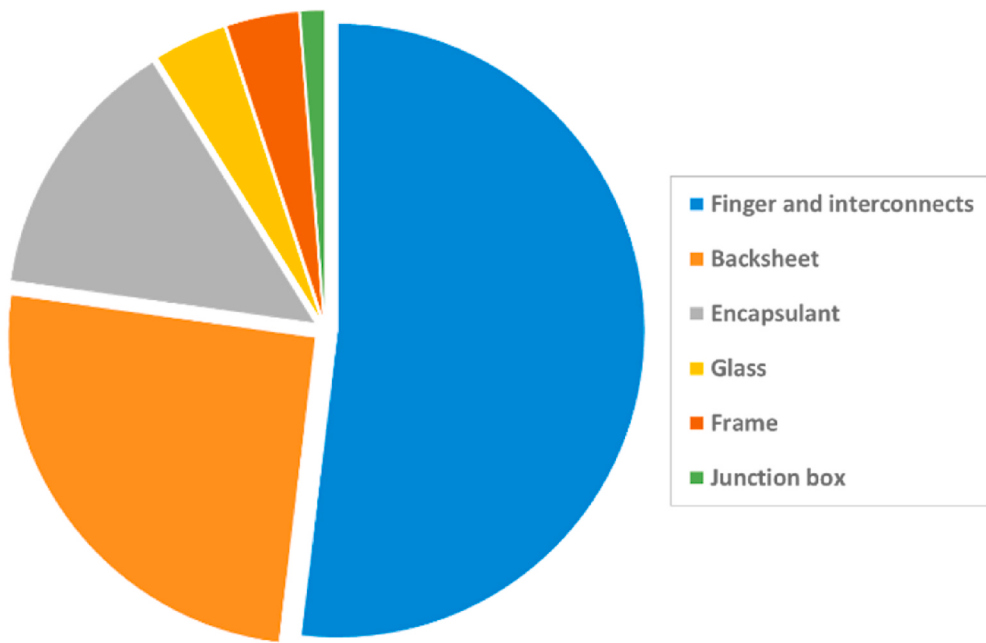


Fig. 1. Occurrence of degradations observed after 22-years in different components of PV modules installed in a composite climate.

Moreover, the current scenario is seeing technological advancements in the field of novel cell metallization architecture from the front-side metallization with continuous rear aluminium back-surface field (Al-BSF). These new technologies include, advanced rear contact designed cells such as; silicon heterojunction technology (HJT), interdigitated back-contact (IBC) and passivated emitter rear contact plus (PERC+) cells, in both mono-facial and bifacial module packaging [4–7]. Even though, these cell architectures are different, it is expected that few degradation mechanisms would be similar to those observed under the front-side metallization with a continuous Al-BSF cell architecture. However, the reason for degradation would significantly depend on the different manufacturing technologies used for integration of the novel metallization into the changed cell architecture. The various factors like

material property and boundary condition provided by different module packaging layers would also impact the occurrence of thermo-mechanical and chemical-based degradation of the interconnects and metallization.

The D & D in PV modules are generally observed in the wafer, metallization, anti-reflective coating, interconnects, and module packaging [8–12]. The metallization and interconnects are essential working components of the module, and are commonly observed to be vulnerable to D & D. Fig. 1 presents the frequency of occurrence of D & D in different components of field-aged PV modules installed in a composite climate for 22 years. Fig. 1 has been adopted from Rajput et al. [11]. It can be observed that finger and interconnect degradations were majorly reported, followed by D & D in backsheet and encapsulant layers. These

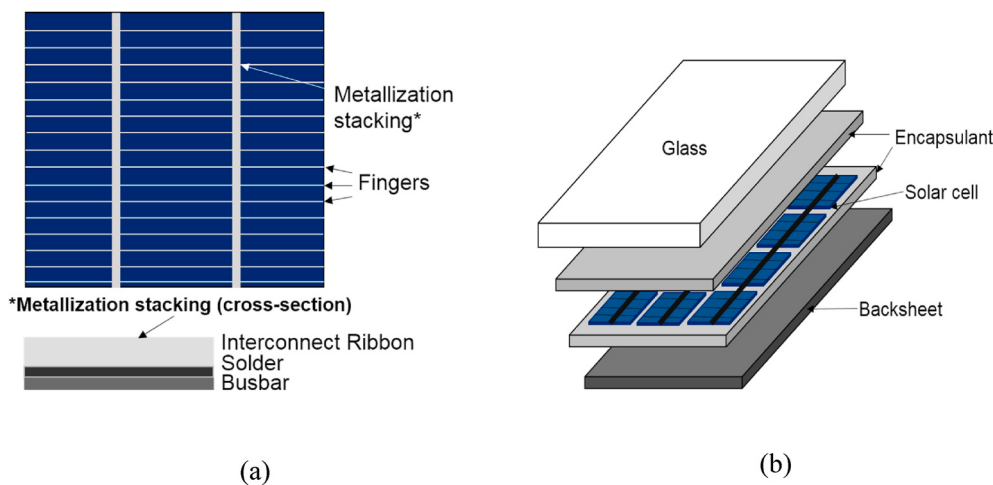


Fig. 2. (a) Schematic of front view of PV cell depicting fingers and metallization stacking and (b) a PV module depicting different packaging layers.

types of degradations are generally reported for modules aged 10 years and above [13]. In addition, various studies have also reported finger and interconnect degradations under different climatic conditions namely, hot and humid, hot and dry, and cold and sunny [14–19]. This indicates that the metallization and interconnect D & D's are relevant in fielded PV modules.

Further, even though recent developments on advancement of cell metallization and interconnect technologies are ongoing, the conventional processes and technologies are still dominantly used. Thereby, a review and analysis on the commonly observed D & D in the commercially utilized cell metallization and interconnects can be useful. Also, the module packaging related defects like EVA degradations, and other cell degradation like, wafer cracks have been well reviewed [20–22]. Thereby, the need for review and analysis of the commonly observed cell metallization and interconnect D & D forms the objective of the present paper.

The defects in PV modules are majorly induced via mechanical, thermo-mechanical, chemical, and photo-chemical modes of degradation in the outdoor environment like hail, dust, gas, moisture ingressions, temperature variations, ultra-violet (UV) irradiance etc. [23–26]. Herein, temperature and humidity are the most common environmental parameters which cause degradation [27,28]. Temperature variation has been reported to induce thermo-mechanical fatigue in the PV module and its components. The cell components including wafer, metallization and interconnects are especially vulnerable to such conditions, owing to differences in thermal expansion, mechanical fragility, and dimension or material properties. Herein, finger breakages, wafer cracks, interconnect breakages and solder bond failures are commonly reported in the outdoor field conditions, and have been discussed in detail in this review [29,30]. Such conditions usually occur due to sudden cloud cover or differences in temperature between day and night in the field. On the other hand, humidity causes degradation due to moisture and gas ingressions through the backsheet and encapsulant, over an extended period of time [31,32]. This often occurs in the hot and humid conditions [33,34]. Such ingressions weaken the interfacial adhesion, which causes delamination and facilitates ingressions paths, leading to multiple modes of chemical degradation in metallization and interconnects, commonly known as corrosion. The multiple types of chemical degradation can induce different modes of electrical loss, irrespective of the final loss in power, such modes have been elaborated in this review. In addition to the environmental factors, inaccuracies and faults at the screen printing, interconnection and soldering process lead to multiple types of D & D in metallization and interconnects, and have been included in detail. The degradation can also be caused and affected by the geometrical design parameters maintained during the screen

printing process [35,36]. Also, defects like shunts under fingers and busbars can form during the printing process [37]. Additionally, sometimes fingers also get broken during the manufacturing process or transportation. Another important factor is the material composition of the silver paste, tin coated copper, and solder alloy, which strongly influence the cell and module performance and reliability [38–40]. These factors indicate the need to ensure care at the cell manufacturing units before the field exposure. The classification of metallization and interconnect defects on the basis of their dominant operating modes can be useful in defect prioritisation, for further planning and mitigation. Further, the understanding of the nuances in operating modes of electrical loss have been elucidated in the present review, which can be useful for increased comprehensibility of the D & D.

The comprehensive analysis of the abovementioned degradation is also facilitated by accelerated environmental tests, to establish the reliability of the freshly manufactured module batches. In this direction, the International Electrotechnical Commission (IEC) have set some indoor environmental standard accelerated tests, which are used for pass or fail qualification of module batches before installation in the field. However, in absence of any other specific application based test, they are used for assessing the reliability of modules against common environmental temperature and humidity variables. In this direction, the IEC 61215 standard has been developed for terrestrial c-Si PV modules. It includes thermal cycle (TC), humidity freeze (HF), and damp heat (DH) test [41,42]. Various defects have been reported in the metallization and interconnects under these tests [43,44]. The detection and quantification of the D & D in metallization and interconnects, observed under the outdoor field and indoor accelerated test conditions, are performed using various characterization techniques. Illuminated current-voltage (I-V) analysis is generally used for evaluating the loss in electrical parameters, however, for identification of the source of faults, detailed diagnostics and defect detection can be performed using destructive as well as non-destructive testing (NDT) techniques. Some common NDT imaging techniques used for defect characterization in finger and interconnects include, electroluminescence (EL), infrared (IR), dark lock-in thermography (DLIT), laser beam induced current (LBIC) imaging techniques etc. [37,39,45–48]. On the other hand, detailed investigation are also performed using various techniques which require destruction of the module like, Fourier transform infrared (FTIR) spectroscopy, scanning electron microscopy-energy dispersive spectroscopy (SEM-EDS), and X-ray photoelectron spectroscopy (XPS) etc. [49–53]. The imaging techniques have immense potential of being exploited effectively for detection and detailed analysis of defects in fingers and interconnects, owing to realizable resolution and sensitivity for imaging of small current carrying components, without destruction of the

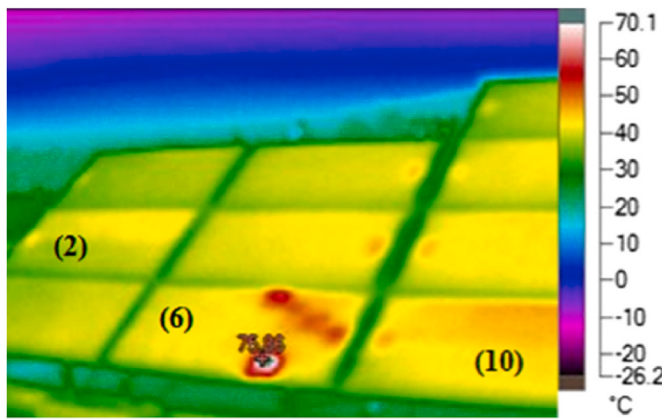


Fig. 3. IR image of a PV array indicating hotspot visible as red spot, due to interconnection failure in the outdoor field [8]. (For interpretation of the references to color in this figure legend, the reader is referred to the Web version of this article.)

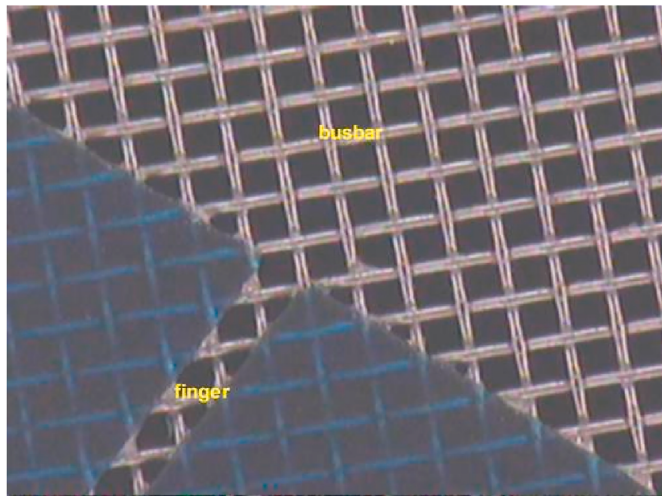


Fig. 4. Visible image of wire mesh used for screen-printing [60].

module. A review and analysis on the different above-mentioned aspects of the metallization and interconnect degradations, including the current trends and developments is essential and beneficial for development of future research in this area. A plethora of papers are present on degradation of other cell and module components, however, not for finger metallization and interconnects.

This paper presents a comprehensive review and analysis on multiple aspects of finger and interconnect metallization including, detection and identification using different characterization techniques, detailed mechanism of degradation, and mode and impact of electrical or other losses. For better comprehensibility, the defects have been classified on the basis of the dominant modes of degradation viz. thermo-mechanical induced, chemical induced, and voltage induced, as well as manufacturing induced defects. The defects have been investigated for the respective modes of electrical loss, and sensitivity to common variable parameters like position, orientation and number of defects by simulation using PSpice circuit simulator, for increased understanding of underlying defect mechanisms and severity. Finally, an in-depth discussion, analysis and suggestion on the different aspects of the reviewed degradations have been elucidated. The information from these discussions can be instrumental for in-depth understanding of these defects, which may further helpful in their prevention and mitigation.

The outline of this paper's contents are as follows. Section 2 provides

the background to metallization and interconnects in crystalline silicon PV cells. The sub-sequent sections of section 3 present a detailed review on the different reported finger and interconnects D & D. The sections are categorised on the basis of major modes of degradation operating in these defects. Section 4 presents an in-depth discussion, conclusions, findings and suggestions on the D & D discussed in the previous sections. It also includes simulation-based results to signify the electrical impact of different finger defects discussed in the previous sections.

2. Front grid fingers and interconnects in crystalline silicon PV cells and modules

The front grid metallization of a crystalline silicon PV solar cell comprises of a grid of silver fingers and busbars, as shown in Fig. 2 (a). The metallization assists in the collection and conduction of current from the emitter layer in the cell. The cells are connected in a series (or parallel) manner for obtaining the desired P_{out} from a PV module. The cells are connected using copper interconnects, which are soldered over the silver busbar. The interconnected cells are packaged in a multi-layered packaged structure, as shown in Fig. 2 (b). The multi-layered structure consists of a low iron glass, adhesive encapsulant (generally EVA) and a polymer backsheet. This packaging protects the cell, metallization and interconnects from external environmental conditions.

The metallization and interconnects are essential working components of a cell, and maintain the overall electrical performance of a PV module. Henceforth, any D & D in them can disturb the electrical and structural integrity of the module. The most dominating electrical parameter affected herein is series resistance (R_{series}), as the fingers and interconnects constitute the current conduction paths in the cell and module. Wherein, high R_{series} is the major mode of degradation, due to different fallacies and defects in these current carrying components. It can be caused due to different factors, via disruption in current, under manufacturing as well as outdoor field conditions like, breakages and interruptions, change in material composition like formation of oxides, migration of conductive materials, loss of adhesion causing high contact resistance, and presence of other defects like solder failure, cell cracks etc. The increase in R_{series} dominantly, reduces the fill factor (FF), and can also impact the short circuit current (I_{sc}) at very large values. These losses lead to reduction in P_{out} , in accordance with Eq. (1) described below.

$$P_{out} = V_{oc} \cdot I_{sc} \cdot FF \quad (1)$$

where, V_{oc} is the open circuit voltage and, I_{sc} is the short circuit current.

In addition to the abovementioned electrical loss mode, the presence of finger and interconnect degradations in the outdoor field, can also cause electrical mismatch within the module, which leads to formation of hotspots [54,55]. In such cases, severe finger defects and interconnect failures causing very high R_{series} , causes decrease in I_{sc} of the cell [56]. This can lead to hotspot heating when one cell or module in a series connected module or string respectively, produces lower I_{sc} in comparison to other cells or modules. The IR image of a module array showing hotspot formation, due to interconnection failure is shown in Fig. 3. In such cases, when the module is short-circuited under outdoor irregular solar illumination conditions, the cell with lowest I_{sc} is forced to operate in reverse bias. This causes the cell to sink large amount of power, causing overheating [57].

The degradation of the fingers and interconnects can also be caused by manufacturing inadequacies due to faults in printing, tabbing and soldering, improper process parameters including temperature conditions, non-optimization of design parameters, material composition etc. In this direction, constant technology improvement is ongoing. However, screen printing process as well as soldered interconnects, remain the commercial and most conventional technologies used in cells and modules. Furthermore, there has been constant improvement in these

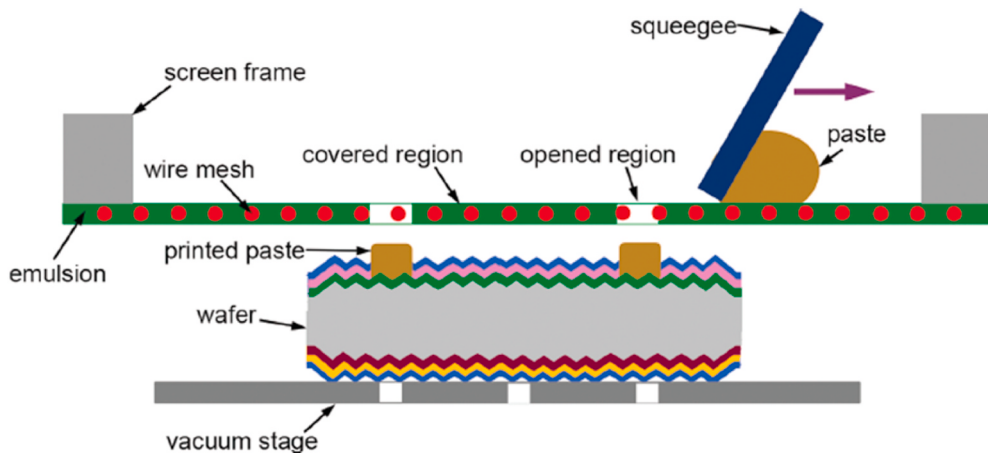


Fig. 5. Schematic of screen printing process on the cell wafer [64].

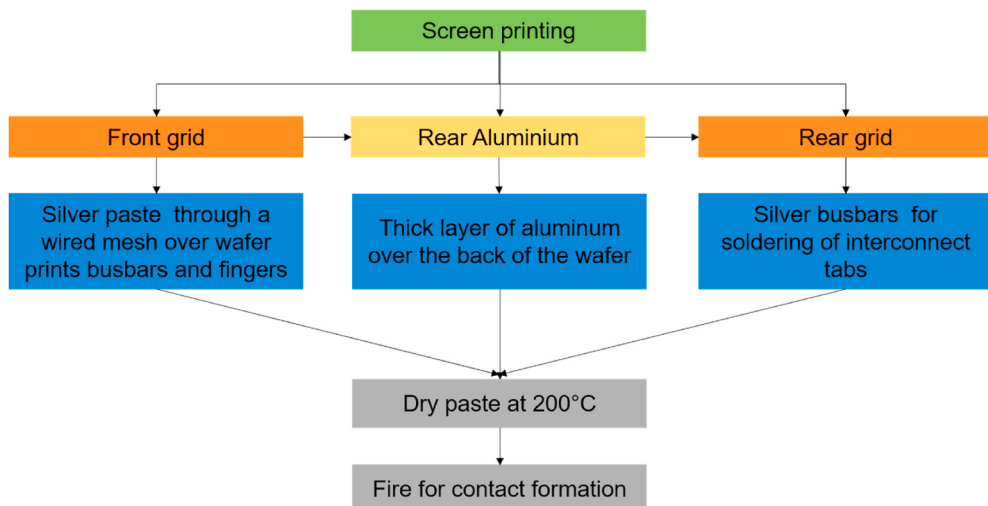


Fig. 6. Schematic depicting screen printing process of metallization on a PV cell.

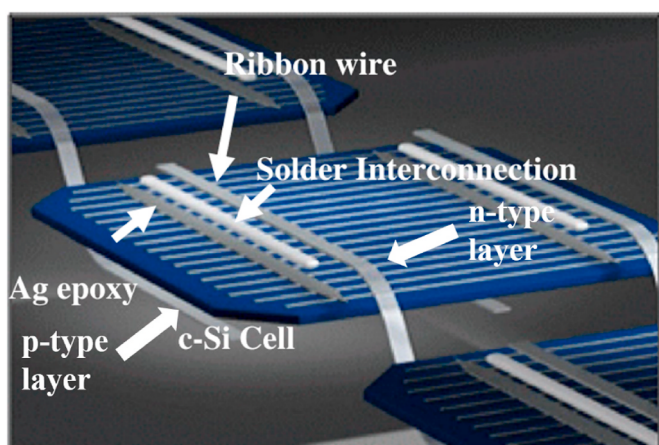


Fig. 7. Schematic of solder interconnection process [65].

existing technologies, for example, changes in silver paste, tin coating of copper ribbon, and solder material chemical compositions for improved efficiency, optimization of design parameters like narrower fingers while maintaining resistive losses, and changes in string design. The screen printing technology is widely used owing to its ease of

implementation on a large scale [58,59]. Wherein, the printer forces silver paste over a wired screen template kept over the front side of the solar cell. The wired mesh consists of a busbar and multiple fingers perpendicular to the busbar, as shown in Fig. 4.

The schematic of the screen printing process is given in Fig. 5. The silver paste seeps through the squeegee and the openings in the wired mesh, and prints busbar and fingers over the wafer. Since, the paste is wet after the previous step it is kept in a dryer at high temperature. Later, the wafer is subjected to a firing process to introduce contact between the printed metallization and wafer at a high temperature. A similar process is performed for printing of aluminum and rear busbar contacts. The process has been summarized in a schematic shown in Fig. 6. The silver paste used in this process contains approximately 90 % silver particles ($\sim 1 \mu\text{m}$). Additionally, glass frits, inorganic additives (Lead, Bismuth, Zinc, Tin, Boron, Aluminum, Manganese, Nickel, and Thorium), cellulose resins, and surfactants are also added to enhance certain properties of the paste [61]. The amount of silver paste required for printing has decreased in the last few years, along with improvement in its conductivity and printability. Some of the mentioned inorganic additives are present in glass frits as oxides. These glass frits enable contact through the anti-reflection coating layer, while ensuring passivation of the silicon wafer [62]. This phase supports the ohmic contact between the silver metallization and silicon wafer [63]. They also help decrease the temperature to avoid mismatch during the firing process, which improves the mechanical strength of the silver-silicon

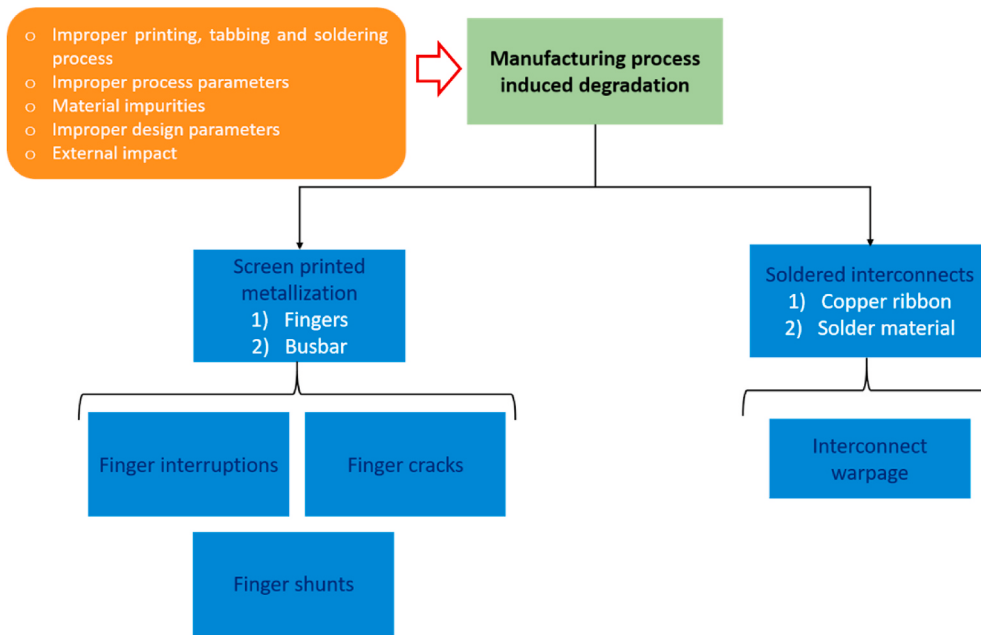


Fig. 8. Schematic of reported manufacturing process induced defects in metallization and interconnects.

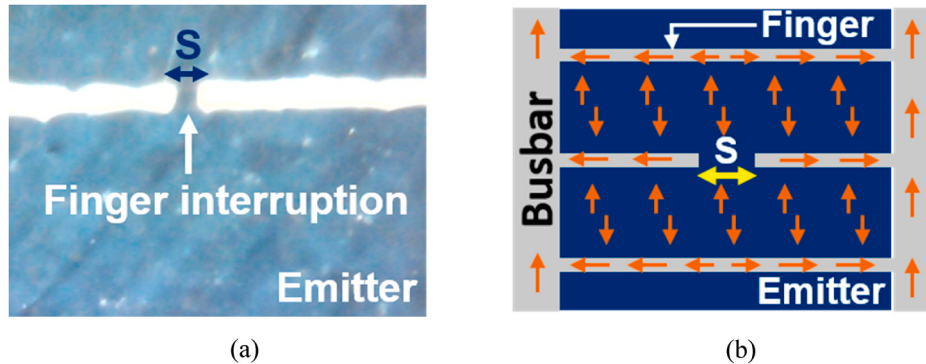


Fig. 9. (a) Visual image of a finger interruption of width S in a PV cell and (b) schematic representing current flow in a cell in presence of a finger interruption.

assembly [61,63,64]. Henceforth, any degradation in these glass frits can lead to reduction in adhesion between the fingers and wafer, as well increase the contact resistance, eventually causing loss in P_{out} .

In the interconnection procedure, a copper ribbon is soldered on the busbar for connecting cells in the module. To make a series connection the n-type layer of the first cell is connected to rear surface (p-type layer) of the adjacent, as shown in Fig. 7. The copper ribbon used for interconnection is typically an oxygen-free high thermal conductivity copper material of width varying between 1 mm and 3 mm and thickness 0.08 mm–0.2 mm. The ribbon used in modules are generally layered with the solder alloy on the surface of a coating thickness varying between 10 μm and 30 μm , typically 20 μm . The conventionally used solder material is an alloy of tin and lead, nowadays many manufacturers use unleaded solder alloys owing to toxicity of lead. The low melting point temperature of tin based solder alloys leads to creep behaviour of the solder layer at nominal temperatures maintained during accelerated TC and field conditions, and hence is susceptible to high temperature changes [12, 54]. The accumulation of strain in the solder joint can lead to its fracture, which can cause de-bonding in the adjacent metallic components, and result in high R_{series} and loss in P_{out} of the module. The proximity of the solder layer to other components like fingers and interconnects, increases the chances of defects in the latter under different modes of solder layer degradation. These defects include finger breakages,

interconnect breakages, and warpage etc.

The impact and susceptibility of metallization and interconnects to degradation in the outdoor field, is also governed by the geometrical design parameters maintained during the manufacturing process. The area covered by the metallization has to be optimized with emitter area available for photogeneration, while maintaining the resistive losses in the cell at minimum. In this regard, a high aspect ratio, viz. height to width ratio of metallization, is generally ensured, to increase the current production while minimizing the shadowing due to metallization, and also optimizing the resistive losses due to low metallization width. However, there are technical and manufacturing constraints, which limit reduction in width of the fingers. Also, finer fingers are more prone to breakages. Henceforth, the degradation aspect to reduction of finger widths should also to be considered. The other aspect is the contact resistance between the finger and silicon wafer, a high contact resistance due to possible adhesion losses or depositions of other low conductivity materials can increase the overall R_{series} and lead to loss in P_{out} . Similarly, in the case of interconnects, multiple reasons can cause loss of contact with the solder or the busbar, which eventually affects the current conduction and collection between cells in a module. The rheology of the material is also an essential aspect which can determine the material quality, herein, the material flow and the chemical composition of the silver paste can be improved to increase the stability

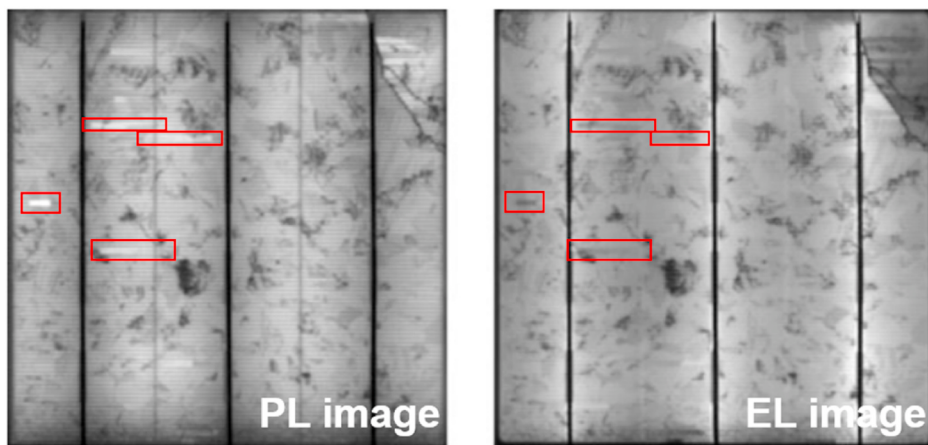


Fig. 10. PL and EL images of a PV cell with finger interruptions [46].

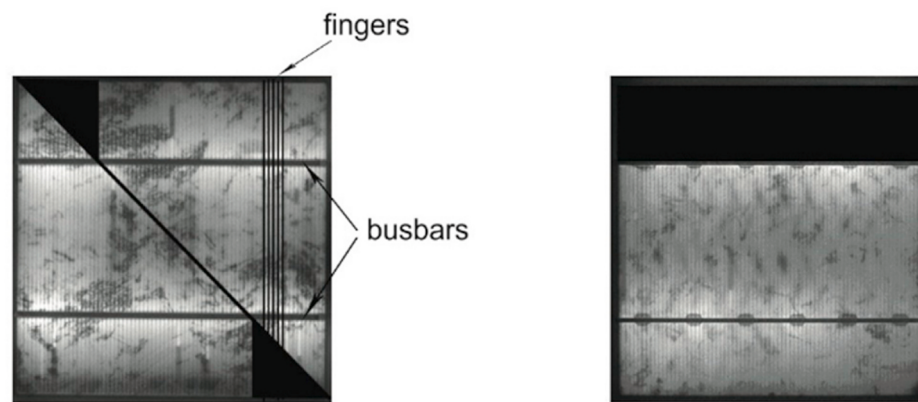


Fig. 11. EL images of cells with wafer cracks with two different orientations [72].

and printability of the paste [66]. The material properties are maintained, while maintaining sufficiently low resistivity of the silver paste. The other dominant design parameter which can be affected in presence of finger breakages and interruptions, is the distance between the two fingers [67,68].

3. Degradations in finger and interconnects

The subsequent sections present a comprehensive review and analysis on different aspects of D & D in finger and interconnects. The sections have been classified on the basis of the major operating modes of degradation viz. manufacturing process induced defects, thermo-mechanical fatigue induced, chemical degradations, and system voltage assisted degradations.

3.1. Manufacturing process induced

The screen printing, tabbing and soldering process can lead to various D & D in the metallization and interconnects. These defects can either be induced during the manufacturing process itself, or evolve in the outdoor field conditions. The different aspects including detection using characterization techniques, mode of electrical loss and current developments on reported defects (Fig. 8) have been discussed in detail in this section.

3.1.1. Finger interruptions

Finger interruptions are commonly reported in finger metallization, which are fabricated using the screen printing process [69]. A visual

image of a finger interruption (of width S) is shown in Fig. 9 (a). These interruptions can occur due to insufficient paste deposition during the screen printing process, or damage from impact during the manufacturing process. The probable causes of interruptions have also been classified on the basis of width of interruption. Herein, any gap S, between 10 µm and 1 mm is due to insufficient screen printing, whereas a gap of more than 1 mm has been attributed to accidental damage during manufacturing process [36].

A schematic of current flow inside the cell with interruption is shown in Fig. 9 (b). The discontinuation in the finger causes the current to travel a longer path from the emitter, thereby causing higher Rseries leading to P_{out} loss. The position of the interruption and number of affected fingers can also affect the electrical loss, which has been investigated and discussed in the subsequent section 4. The electrical impact of finger interruptions has also been shown to depend on its location in respect of the busbar. It is also been reported that impact of such defects increase with the silver resistivity and amount of interruptions [59].

These interruptions are small, and often not visible to the naked eye. Henceforth, EL imaging technique is found to be effective for identification of such interruptions during the manufacturing stage [46,70]. Tseng et al. have devised an automated classification system using EL imaging to identify the finger interruptions from other type of defects, during the manufacturing process [69]. Even though, EL imaging is more commonly used for the purpose of identification of these defects, Zafirovska et al. have presented the application of contactless, line scan photoluminescence (PL) imaging for detection of finger interruptions [70]. The finger interruptions have been marked in red in the PL and EL

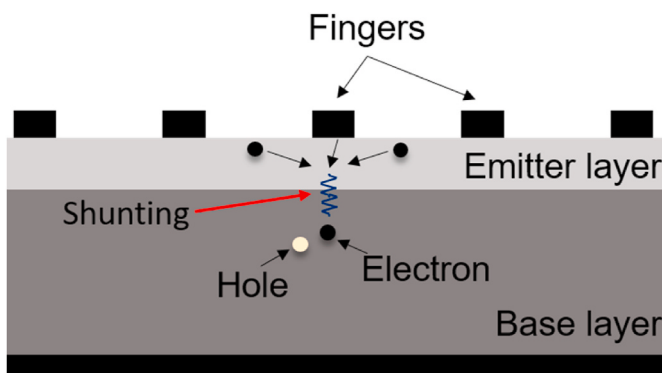


Fig. 12. Schematic representing the finger shunting phenomenon in a cell.

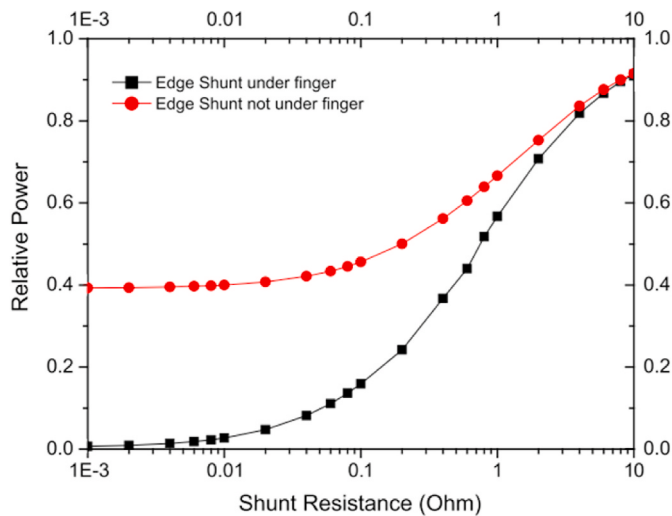


Fig. 13. Relative power with shunt resistance, for a finger and non-finger shunt [75].

images shown in Fig. 10. Herein, the substantial advantage of line scan PL imaging has been presented for differentiation between the similar appearing defects, which cause high R_{series} (like, finger interruption) from the dark regions of high recombination in the EL images.

3.1.2. Finger cracks

Finger cracks are induced when a wafer crack cuts across the finger [71]. An example of such cracks, causing electrically separated regions in the EL images is shown in Fig. 11. The EL imaging technique is the only reported technique for the detection of this defect type. Also, Chen et al. have devised an automatic crack detection system using EL imaging technique, which can be utilized for finger crack detection in cells [43].

Such cracks lead to multiple finger breakages in the cells however, the mode of electrical loss as well as the defect severity will depend on

the orientation of the cell to cell crack. This vital aspect of severity of finger cracks has been investigated in section 4. The cracks can affect the R_{series} and I_{sc} of the cell. The cracked regions can also facilitate moisture and gas ingressions, which can further lead to metallization and interconnect corrosion.

3.1.3. Finger shunts

Finger shunts are an alternative low resistance path for current conduction, due to direct contact of silver paste with the base layer or back contact [73,74]. A schematic representing the finger shunting phenomenon in cells is shown in Fig. 12. Such shunts are generally process induced, and can be formed during the fabrication process due to scratches, wafer cracks, or improper metallization contact [75,76]. During the screen printing process, the silver paste can seep through the emitter causing a Schottky-type shunt [77]. Such shunts are also reported at regions of the cells wherein the emitter layer is missing due to mechanical breakages of texturization or dust particles during junction formation. In other cases, severe shunts are also observed in the presence of existing wafer cracks, leading to direct contact of silver paste with the back contact [74].

Shunts cause degradation in the cell performance, and affect the overall efficiency of the PV module by reducing the FF. Fig. 13 depicts the severity of finger shunt, in respect of a shunt at another location in the cell. The relative power represents the ratio of power of cell in presence of shunt, to that in absence of shunt. It can be seen that the relative power of finger shunts are less than other shunt location, representing higher loss in P_{out} due to finger shunts. Shunts are especially dangerous in the outdoor field, where shunted cells can come under high reverse bias due to shading conditions [78]. Here, hotspots can cause irreversible damage to the cell and module [79].

Roy et al. have utilized the combination of EL and DLIT imaging to

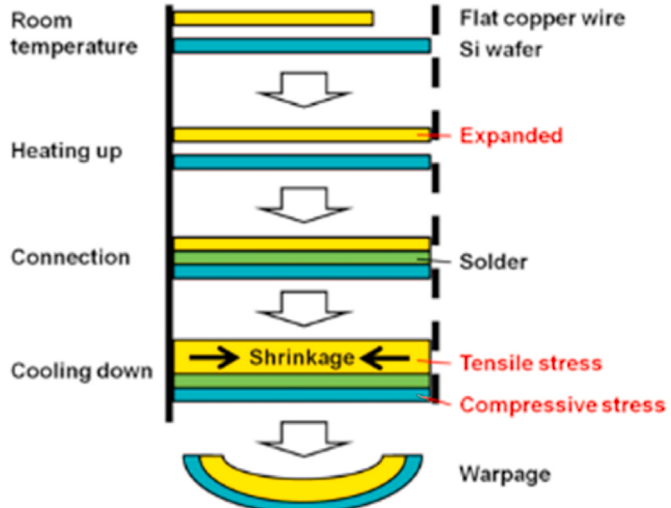


Fig. 15. Schematic representing warpage phenomenon during the interconnection process [81].

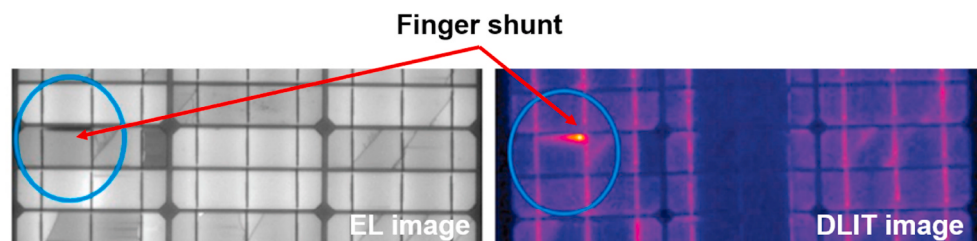


Fig. 14. EL and DLIT image of a portion of PV module, depicting finger shunts [37].

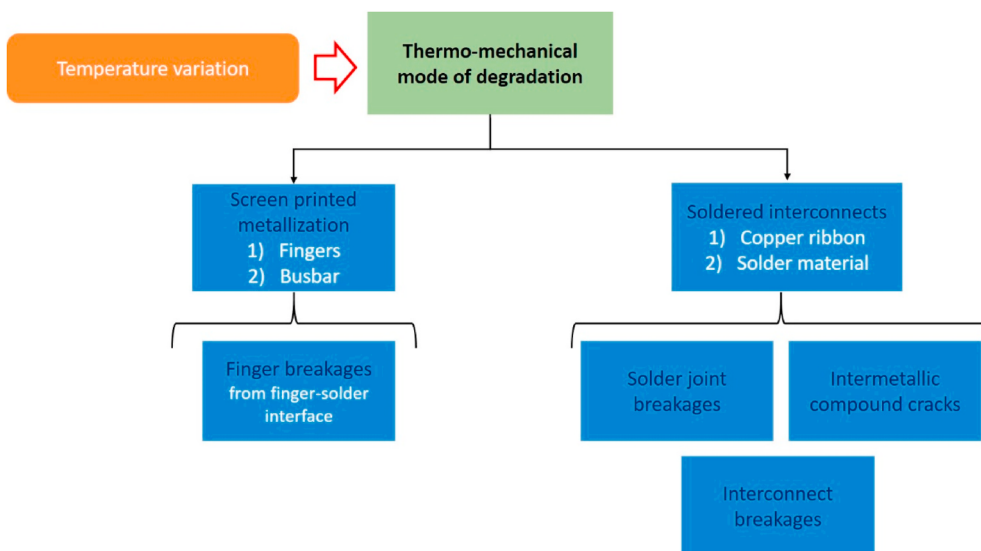


Fig. 16. Schematic of reported defects in metallization and interconnects due to thermo-mechanical mode of degradation.

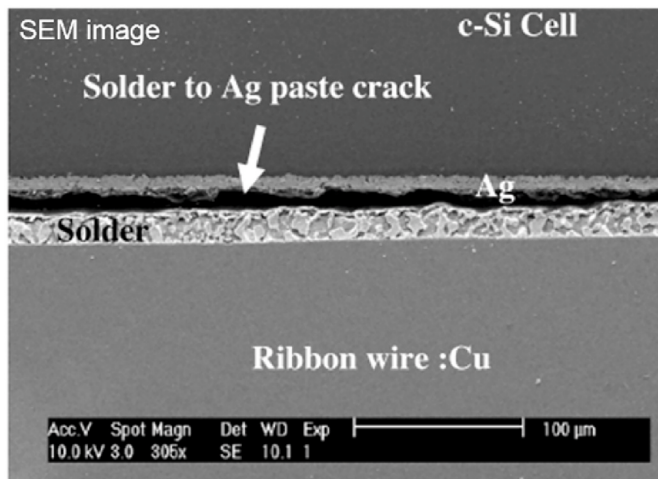


Fig. 17. SEM image indicating solder joint crack in an outdoor exposed module [65].

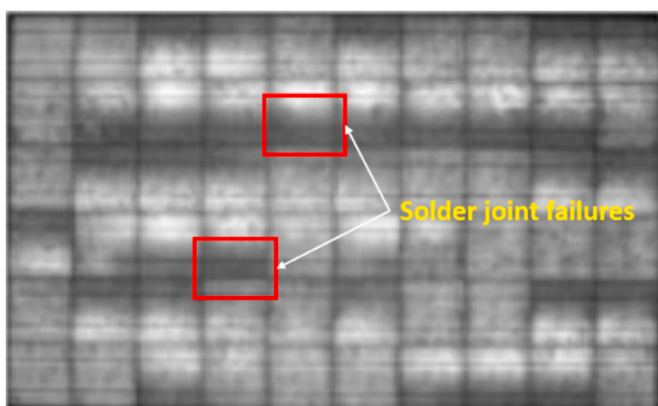


Fig. 18. EL image of a PV module depicting solder joint failures under TC test [95].

identify the location as well severity of finger shunts in PV modules. The finger shunt appears dark in the EL image, and bright along the finger in the corresponding DLIT image, as shown in Fig. 14. They have also compared the impact of finger with busbar shunts, which are also made of silver paste. Herein, the latter have been reported to be more severe due to higher current density in them [37]. In addition, micro-structural characterization techniques like SEM-EDS, and LBIC imaging have also been reported for in-depth analysis of finger shunts [37,73].

3.1.4. Cell and interconnect warpage

Cell and interconnect warpage have been reported during interconnect tabbing process due to the bowing effect [80]. It is the deformation of the cell due to the differences in coefficient of thermal expansion (CTE) between the adjacent components. The schematic of the warpage phenomenon is shown in Fig. 15. The cell and soldered ribbon are heated together during the tabbing and stringing process. The copper ribbon has higher CTE than the silicon wafer, hence, expands more than the wafer during the heating period in the soldering process. However, during the cooling cycle the ribbon experiences tensile stress while the wafer experiences compressive stresses, hence leading to the warpage of cell and ribbon [81]. This warpage can lead to wafer and interconnect breakages. It has been reported that thinner wafers have more chances of warpage. It is advised to use a ribbon with low value of CTE closer to silicon to reduce the stress on the wafer [82].

3.2. Thermo-mechanical fatigue induced degradation

Thermo-mechanical fatigue is induced due to difference in the CTE between the different components of the PV module, under transient temperature variations [54]. The fatigue leads to accumulation of strain, which can cause cracks and breakages in the metallization and interconnects, and disturb the electrical continuity of current collection and distribution in the PV cell. The TC test as specified under IEC 61215 is often used for inducing thermo-mechanical fatigue in PV modules [83]. The commonly reported defects in metallization and interconnects under thermo-mechanical fatigue are given in Fig. 16. Herein, finger, solder joint and interconnection breakages are commonly observed [55, 84,85]. Such defects dominantly can cause an increase in the R_{series} , which eventually leads to loss in P_{out} . It may also lead to mismatch in cells, due to non-uniform temperature distribution [86]. Some other factors apart from the dominant thermo-mechanical fatigue which may cause similar degradation modes are vibration, mechanical shock, and thermal aging [45,87].

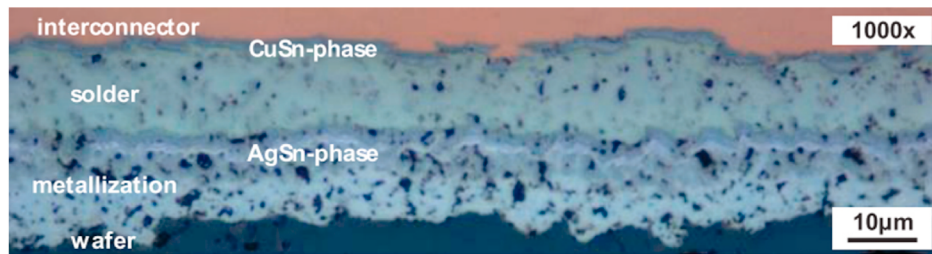


Fig. 19. Microscopic image of IMC formation under aging test [107].

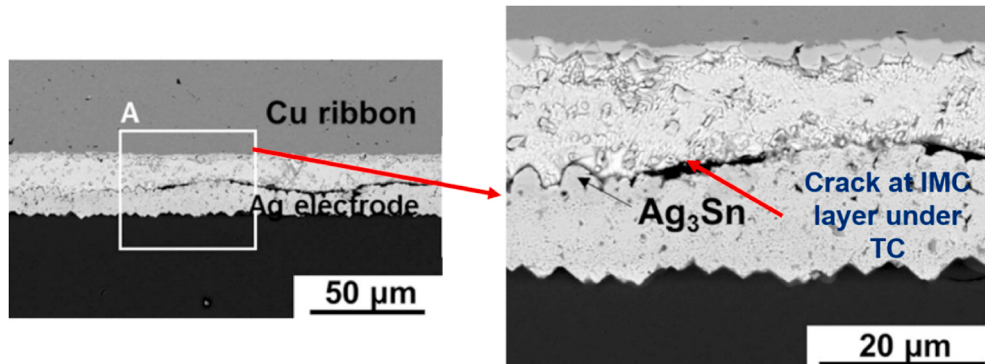


Fig. 20. SEM image of crack in IMC layer at finger interface, under TC test conditions [108].

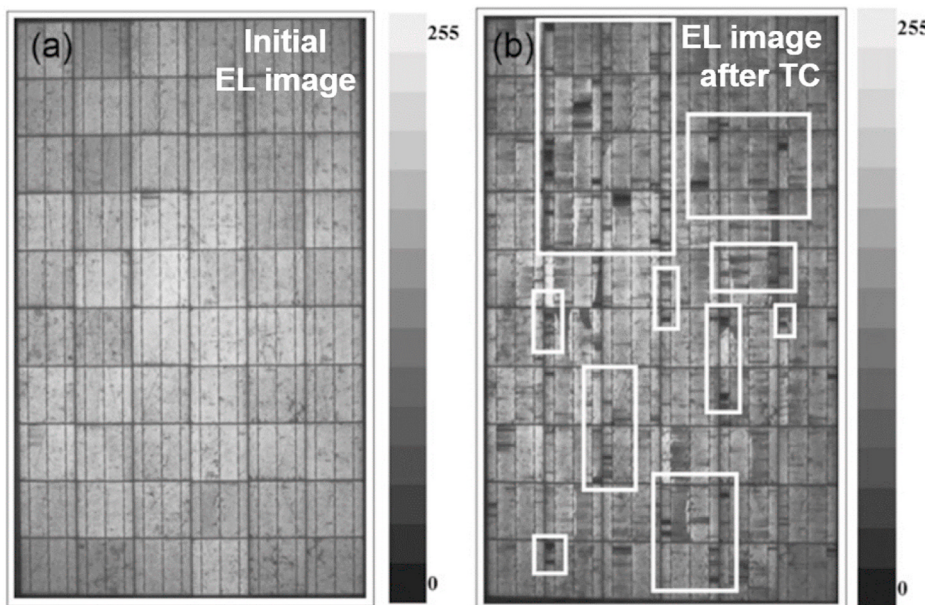


Fig. 21. EL image depicting finger breakages in module under TC test [45].

3.2.1. Solder joint breakages

The solder layer used in PV modules facilitates a robust mechanical and electrical connection between metallization and interconnects. Hence, it is desirable that the solder material remains unaffected during the manufacturing process and the outdoor environmental conditions. However, the solder bonds are vulnerable to breakages [88–90] due to its creep property. This material property is a time-dependant plastic deformation, under thermal stress [91–94]. Fig. 17 shows a SEM image indicating a solder joint crack in an outdoor exposed module. Thermo-mechanical fatigue and thermal ageing are two most extensive mechanism that can lead to solder joint failures [83].

The solder bond failures like cracks, can be identified in the EL images, as symmetrically decreased EL intensity on both sides of the busbar due to reduced current injection, as shown in Fig. 18. The understanding of signatures in EL images can be useful to differentiate between different defects in metallization and interconnects.

The thermo-mechanical fatigue response of PV modules is generally investigated using finite element modelling since, it is complex to calculate the localised stresses and strains in a packaged module [96–98]. The loading condition in such simulations is carried out under the TC test specified under IEC 61215 standard [41,42]. The solder joint breakages can also lead to finger breakages and interconnect breakages,

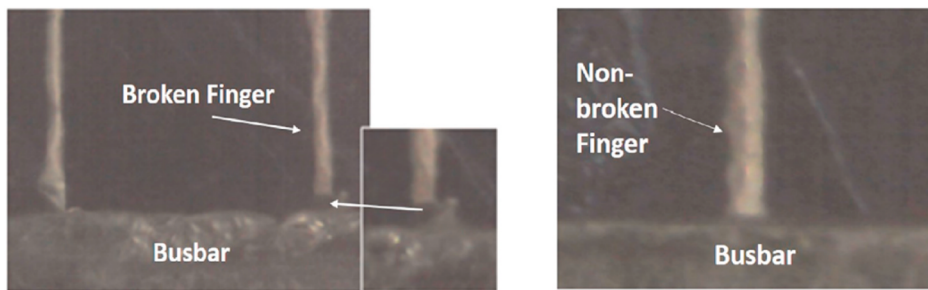


Fig. 22. Microscopic images showing broken and non-broken fingers from ribbon-finger junction [39].

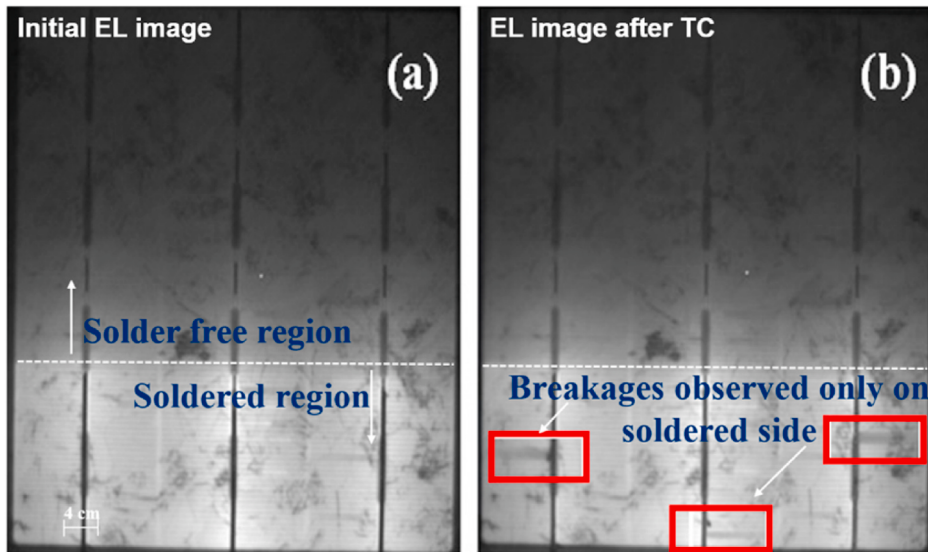


Fig. 23. EL images before and under TC test on a partially soldered cell [85].

as they share common interfaces.

3.2.2. Intermetallic compound cracks

Intermetallic compounds (IMC) are formed due to diffusion of copper and silver from the adjacent components into the solder joints at elevated soldering temperature. The IMC formation takes place at the ribbon and metallization interface [99–101]. The microscopic image in Fig. 19 shows the formation of Cu₃Sn and Cu₅Sn IMC's at the copper ribbon interface, and Ag₃Sn IMC's at the silver busbar interface. After solidification, these IMC's grow due to solid-state diffusion for an extended duration. Generally, the IMC's are brittle and may break at applied stress [102,103]. Also, excessive IMC's growth degrades mechanical properties of a solder joint [99]. The impact of IMC layer formation at the interface is associated with increase in R_{series}, leading to P_{out} loss via decrease in FF [104–106].

The breakage at the busbar-solder interface is the most dominant defect under formation of IMC. The chances of such degradation increase under accelerated testing conditions like TC test. An example of crack formation at finger interface in the IMC layer, under TC conditions is shown in Fig. 20. In this case, the degradation mechanism is due to diffusion of tin into metallization, leading to swelling in the porous metallization, which tends to break under application of stress. This behaviour has been reported to be more in case of leaded solder alloys, in comparison to lead free alloys [107].

It has been reported that the addition of silver to leaded solder alloy, refines the grain structure of alloy under thermal ageing conditions, which reduces the risk of IMC cracks [109,110]. In this direction, new solder alloys have been researched to improve the reliability of IMC layer in the cells [104,105].

3.2.3. Finger breakages

The finger metallization can crack at different positions along its length, which can determine the cause of the breakage. Herein, any discontinuation away from the ribbon-finger junction can be attributed to a manufacturing fallacy. However, finger breakages in the field or under TC conditions are observed to originate from the ribbon-finger junction. Fig. 21 shows EL images of modules before and after TC test, depicting formation of dark rectangular regions or finger breakages from the ribbon-finger junction. A visual image of broken and non-broken finger in respect of ribbon-finger junction has been shown in Fig. 22.

However, breakages emanating from the ribbon-finger junction have been attributed to thermo-mechanical fatigue, owing to the proximity to the solder layer, which is susceptible to temporal thermal variations. Hence, the ribbon-finger junction has also been synonymously termed as the finger-solder interface, indicating the actual source of such breakages. It has been reported that, finger breakages under TC test conditions are only observed from the finger-solder interface [111]. For this purpose, a partially soldered cell was subjected to TC's, and breakages were observed only in the soldered region. This has been demonstrated in the EL images shown in Fig. 23. The breakage in fingers can give rise to increase in R_{series}, which affects the FF, and causes loss in P_{out} [47].

Kumar et al. have simulated the effect of TC parameters, wherein the effect of ramp rate, and dwell periods have been isolated via damage accumulation at the finger-solder interface [84].

3.2.4. Interconnect breakages

Interconnect breakages are one of the most reported failures in outdoor installed crystalline PV modules [65,112,113]. A visual image of an interconnect breakage is shown in Fig. 24. Its main mode of



Fig. 24. Visual image of interconnect breakage in a PV module [8].

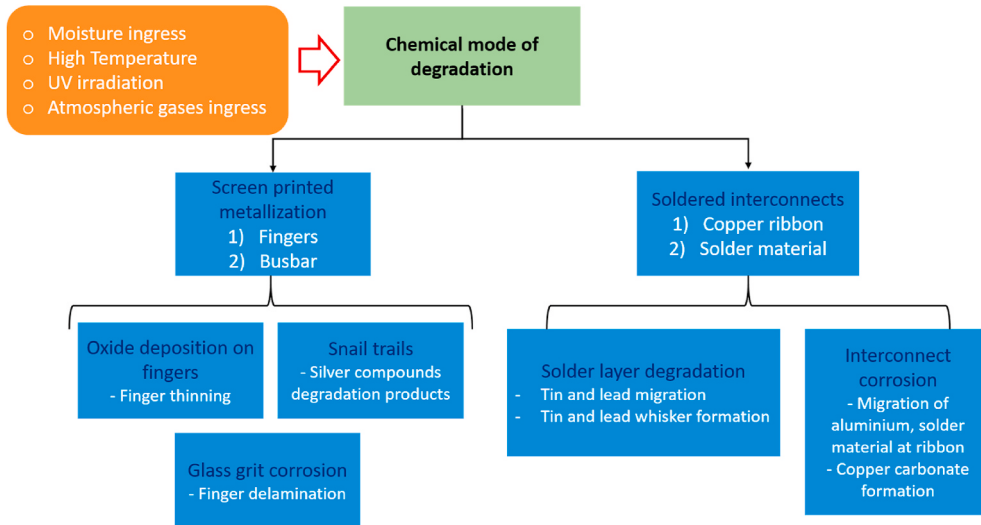


Fig. 25. Schematic of reported chemical degradations in metallization and interconnects.

degradation is due to thermo-mechanical fatigue, owing to differences in CTE of solder joint interconnection of the ribbon with the wafer [55, 114].

Existing conditions offered due to poor soldering and strain accumulation at the ribbon kink between two cells can also lead to such breakages under thermal fatigue conditions [8, 96]. Such breakages have also been reported to cause finger breakages and interruptions at the busbar edges [115]. They have been reported as the dominant reason for increase in R_{series} , in PV modules under outdoor conditions [116].

3.3. Chemical modes of degradation

Chemical induced degradations are commonly observed in hot and

humid areas [8, 117, 118]. The moisture and gases generally enter through the rear of the module, and move laterally over the available cell space [9, 52]. Such conditions are generally simulated indoor, using accelerated DH test [41, 42, 119]. Consequently, multiple degradation products have been reported in literature. A flowchart depicting different D & D reported due to chemical mode in shown in Fig. 25. These defects are commonly detected and characterized using destructive analysis. Such defects dominantly can lead to multiple electrical mode losses, and cause an increase in the R_{series} , which eventually leads to loss in P_{out} .

3.3.1. Silver oxide depositions

Silver metallization corrosion has generally been reported due to

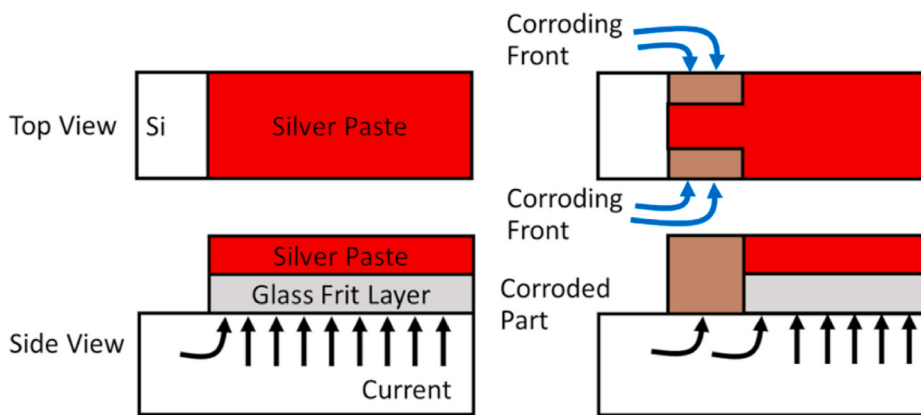


Fig. 26. A schematic representing the finger thinning phenomenon [121].

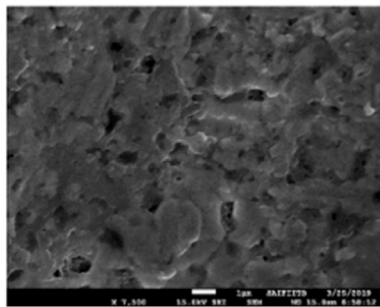
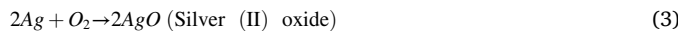
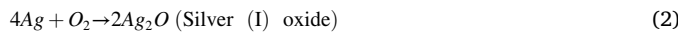


Fig. 27. SEM and EDS analysis finger indicating formation of silver oxide, under DH test [39].

formation of silver oxide over the fingers [120]. The phenomenon has also been termed as finger thinning [121]. Wherein, they have defined it as reduced thickness of the fingers, or reduced cross sectional area of fingers which increase the local R_{series} , and lead to reduced P_{out} [122]. A schematic representing the phenomenon of finger thinning has been shown in Fig. 26. Such depositions have generally been seen under DH test conditions.

The concentration of oxygen diffusion into the module increases at high temperatures. Such conditions are found in the DH test [123]. Herein, the silver and oxygen form silver oxides (2-3). The presence of these oxides have been established using SEM and EDS techniques, as shown in Fig. 27. The equation is as follows [39,120]:



These oxides are deposited on the finger metallization as light to dark brown compounds. Kim et al. have mentioned a thickness of this layer in the range of 10–20 Å [120]. Kumar et al. have reported a signature pattern for identification of silver oxide using combination of EL and DLIT imaging techniques [39]. The pattern can be seen as dark areas in DLIT as well as EL images, at the edges or near the pre-cracked regions, as shown in Fig. 28, where diffusion of moisture and gases through the backsheet was possible.

3.3.2. Glass frit corrosion and finger delamination

Another type of corrosion being reported is the degradation of glass frits found at the interface of fingers and silicon wafer [124]. These glass frits (generally, PbO based borosilicate glass) are found in the silver paste alloy used to screen print fingers and busbars. They enable the contact formation between the emitter layer and silver paste during the firing process, by burning through the ARC coating (SiN_x) [61].

However, authors have detected a gap beneath the silver finger using AC impedance signal and I-V characteristics of cells [125]. These were found in modules from DH test condition. Also, this type of degradation is reported in the presence of an acetic acid environment, found during EVA discoloration process [126]. It is commonly known that EVA degrades due to UV irradiance and moisture, and produces acetic acid by-product [20,127,128].

The glass frits or PbO ionizes to Pb^{2+} or PbOH^+ under such acidic conditions offered by acetic acid. The ionized lead migrates or elutes from the interface leading to loss in contact between the emitter layer and finger, as shown in Fig. 29 [49,129]. This loss in adhesion at the finger interface is also termed as finger delamination, as shown in Fig. 30 [121]. The remaining portion of the glass frits becomes vulnerable to corrosion under the action of moisture and gases. These two effects lead to increase in the R_{series} of the cells and module.

In addition to the PbO , Bismuth is also used as a glass phase in the silver paste. It has been reported that the solder layer above the busbar can react with the Bismuth cations, thereby disrupting the glass network and causing finger delamination [130].

3.3.3. Solder material corrosion

The solder layer material also degrades due to moisture and gases ingress, due to galvanic corrosion [50,108]. Such defects have been reported under both DH and outdoor environmental conditions [54]. In this type of degradation, the material with the lowest oxidation potential has a higher probability of getting corroded at a faster rate. The oxidation potential for Sn/Sn^{2+} and Pb/Pb^{2+} is -0.136 V and -0.126 V respectively, on the other hand the potential of Ag/Ag^{2+} and Cu/Cu^{2+} are $+0.799$ V and 0.337 V respectively. Hence, tin and lead tend to corrode at an accelerated rate, in presence of electrolyte, and deposit over silver and copper [120]. The displacement of solder material under DH test has been shown in Fig. 31 [131].

The tin and lead deposition can occur at different location at the PV cells. Few authors have reported the deposition at the top of the silver fingers, as shown in Fig. 32 [108,132]. This will not significantly affect the current conduction within the fingers. However, due to the displacement of the solder material from the underneath the ribbon, the current flow from the busbar to the copper ribbon would be affected, causing loss in P_{out} .

Kumar et al. have proposed another location of deposition using the information obtained from the EL imaging technique. Wherein, inhomogeneous and randomly located signature patterns were observed in the EL images, generally away from the busbar (Fig. 33).

The location of these patterns suggested an obstruction to lateral current movement from the finger to emitter layer. This information along with the SEM-EDS analysis was used to identify the exact location as the finger-wafer foot or interface. The extent of degradation for this location will be more than that over the finger. This mechanism has been

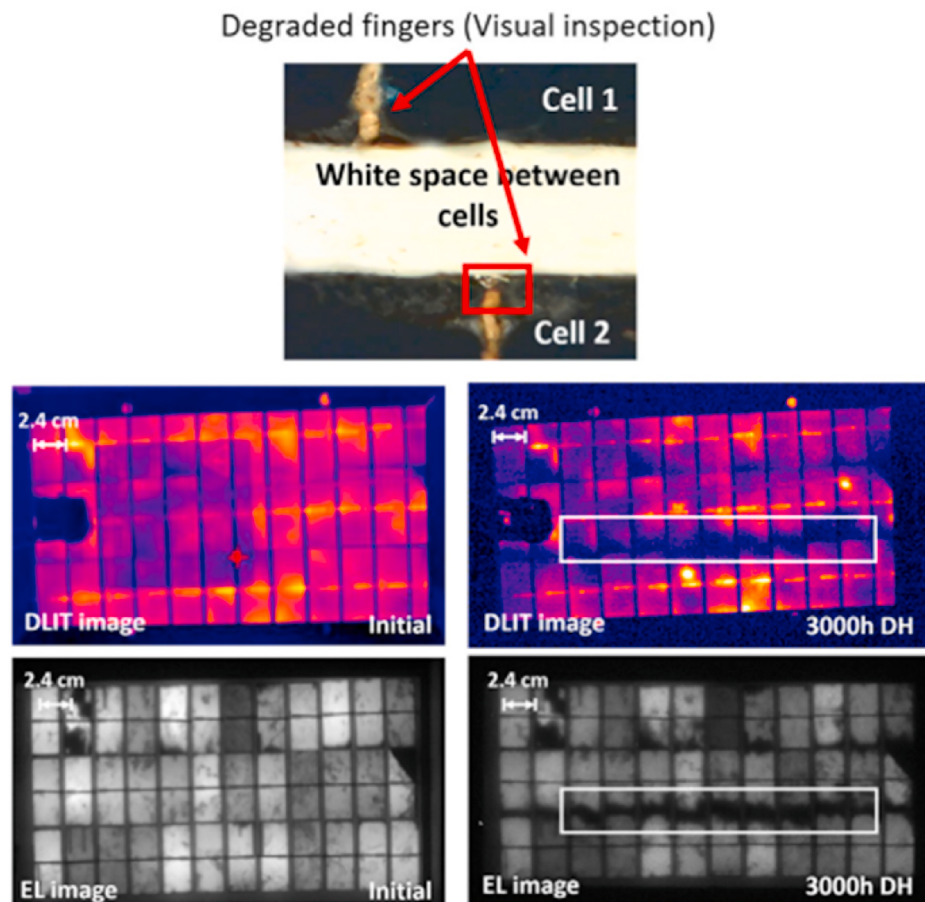


Fig. 28. EL and DLIT images of a module depicting signature pattern of silver oxide formation [28].

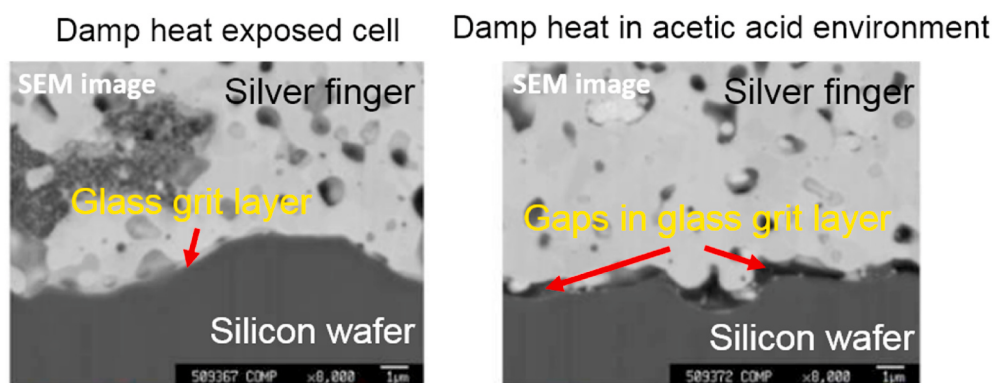


Fig. 29. SEM image showing gaps in glass grit layers in an acetic environment [125].

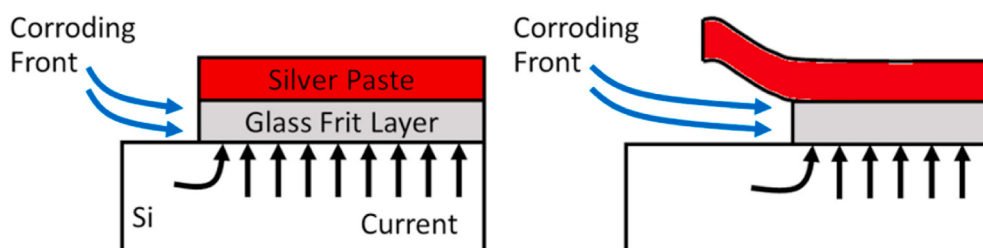


Fig. 30. A schematic depicting the finger delamination phenomenon [121].

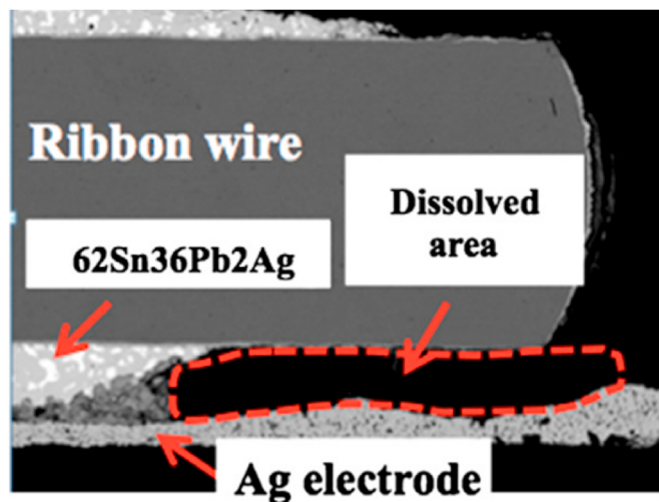
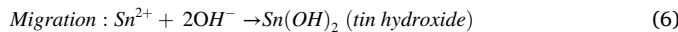
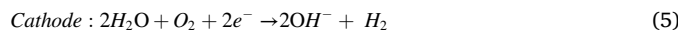


Fig. 31. SEM image showing the displacement of solder material from underneath the ribbon [131].

described in Fig. 34. The equation is given below [39]:



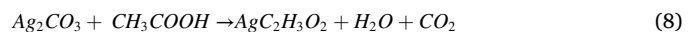
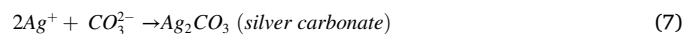
The tin and lead material are also reported in form of whiskers from the SEM images. These whiskers are needle like structures, which can disturb the current conduction and lead to reliability issues. Such issues of whisker formation have also been reported in other microelectronics [133]. The presence of tin whisker has been reported at the busbar interface as well as at the finger-wafer interface. This indicates the migration of tin from the solder material below the ribbon [39]. On the other hand, presence of lead whiskers on the surface of the finger has also been reported [132]. These whiskers are reported to be from the glass frits used in the silver fingers. The whiskers are reported to further form some compounds, which cause increase in local R_{series} . Peike et al. have shown that the needles are found in the top as well as rear of the finger, as shown by the SEM-EDS analysis in Fig. 35. The needles have

been reported in form of lead acetate salt formed under the action of acetic acid evolved during the EVA discoloration process [119].

3.3.4. Snail trails

Snail trails (or snail tracks) appear as darkened or discoloured fingers, reported within just a few years of outdoor exposure [134]. It has been reported that the snail tracks are assisted by micro-cracks or are found at the edge of the cell [51,82,135–138]. These regions allow diffusion of atmospheric gases through the backsheet. Also, the susceptibility of snail trail formation has been associated with the combination of chemical properties of encapsulant and backsheet material used for packaging in the PV module [136,139]. Fig. 36 shows visual images of finger discoloration observed at the edges of a cell, and its imprint on an EVA film separated from the cell.

Degradation products have been identified mainly using different micro-structural characterization techniques like, transmission electron microscopy (TEM), SEM-EDS, Raman spectroscopy. Herein, silver carbonate, silver phosphate and silver acetate are reported as degradation products due to snail trails [139,140]. In addition, silver sulphide has also been observed under DH test conditions [138]. Amongst these, silver carbonate is the most commonly reported degradation products of snail trails [140,141]. The EDS analysis indicating formation of silver carbonate is shown in Fig. 37. The equation is given below [142]:



However, a more recent study indicates that snail trails have less impact on the overall performance of PV modules. The study also shows that there is no relation between snail trails and micro-cracks, which is contradictory to earlier reported works. Also, no traces of corrosion were found on the finger below the snail trail. However, the silver oxide was found on the EVA of the affected modules [143].

3.3.5. Interconnect corrosion

Interconnect corrosion have been reported in outdoor aged modules [8,11]. The ribbon is particularly vulnerable to moisture and gases ingressions through the backsheet. The ribbon can also experience loss in adhesion, due to the vulnerability of the solder layer in presence of moisture. A visual image of interconnect corrosion in an outdoor installed PV module is shown in Fig. 38. Such corrosion at the ribbon can affect the R_{series} of the cell and module [65,121].

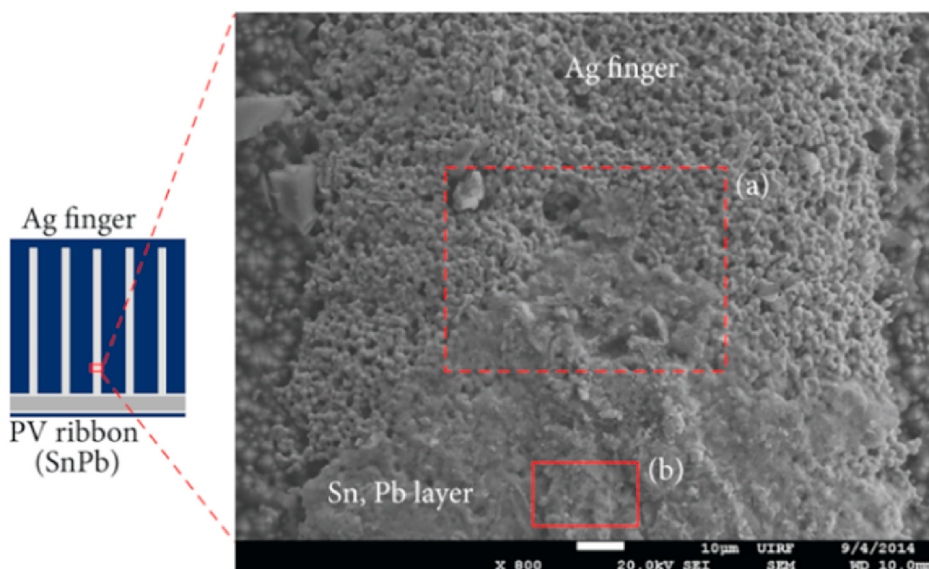


Fig. 32. SEM images showing deposition of solder material over the finger [108].

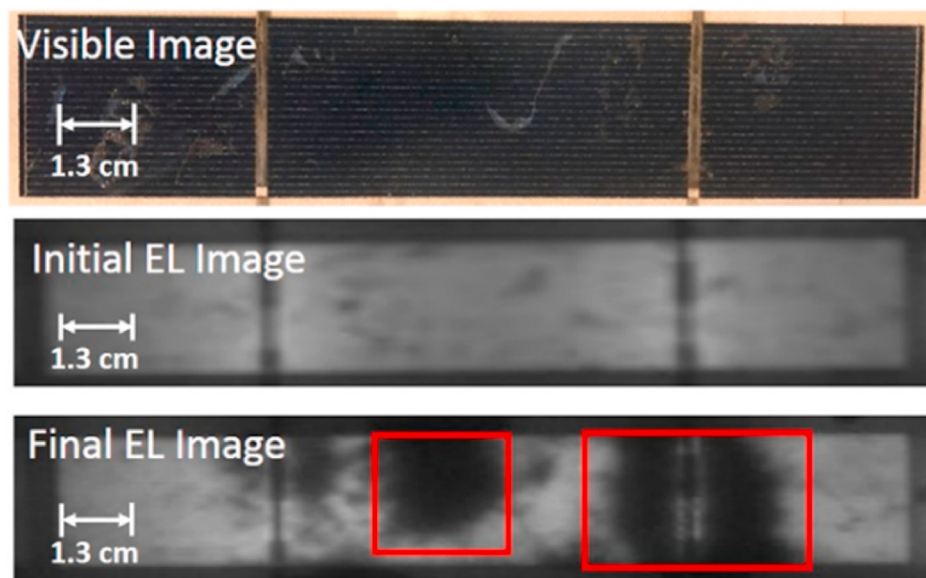


Fig. 33. EL images indicating signature patterns of tin migration in a module [39].

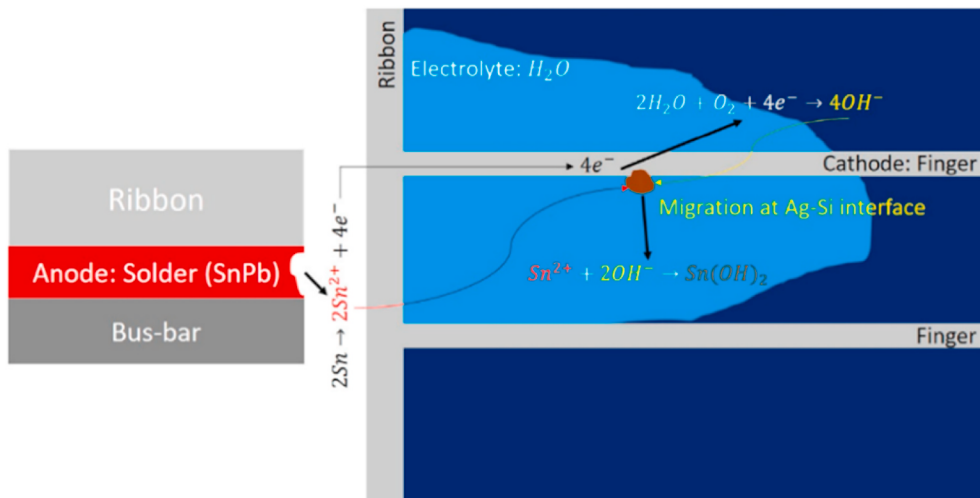


Fig. 34. Schematic of tin migration at finger-wafer foot [39].

The corrosion at interconnects have been described by various mechanisms. Huang et al. have discussed formation of a yellow top coating on the surface of ribbon under outdoor exposure. This has been reported as surface oxidation, and does not affect the current conduction in the cell [144]. Kumar et al. have discussed the migration of aluminium, and solder material as oxides, at the rear of the ribbon in multiple modules under investigation, as another mechanism of ribbon corrosion under humid conditions [39]. In this type of degradation, the overall EL intensity across the modules are reported to decrease. The metal oxide at the rear of ribbon obstruct current conduction into the busbar through the solder layer, causing a high R_{series} path. The formation of copper carbonate visible as greenish deposition has also been reported [39]. An International Energy Agency (IEA) report has also stated that acetic acid affects the copper core and its tin coating resulting in a green copper acetate pattern [2].

3.4. System voltage assisted degradation

The modules are connected in an array in the outdoor field. The system voltage developed across the array is high, and can cause

different degradation modes within the cell and module.

3.4.1. PID assisted delamination at fingers

Potential induced degradation (PID) has also been reported to cause delamination at the encapsulant and cell interface particularly at the fingers [145]. An example of finger delamination in the field is shown in Fig. 39.

The formation of delamination has also been simulated in the laboratory conditions using a PID stress test, comprising of a combination of DH test and voltage stressing under high humidity conditions [145]. Delamination has also been observed around the fingers and busbar in such tests. The factors causing this type of delamination under the stress test have been attributed to DH test causing loss in adhesion strength [146]. Further, the negative potential in the test cause accumulation of sodium form the glass at the cell surface, which further reduces the adhesion [147,148]. Also, the humidity and voltage can cause electrochemical reactions via dissociation of water which releases by-products such as bubbles and cause EVA delamination around the fingers [149].

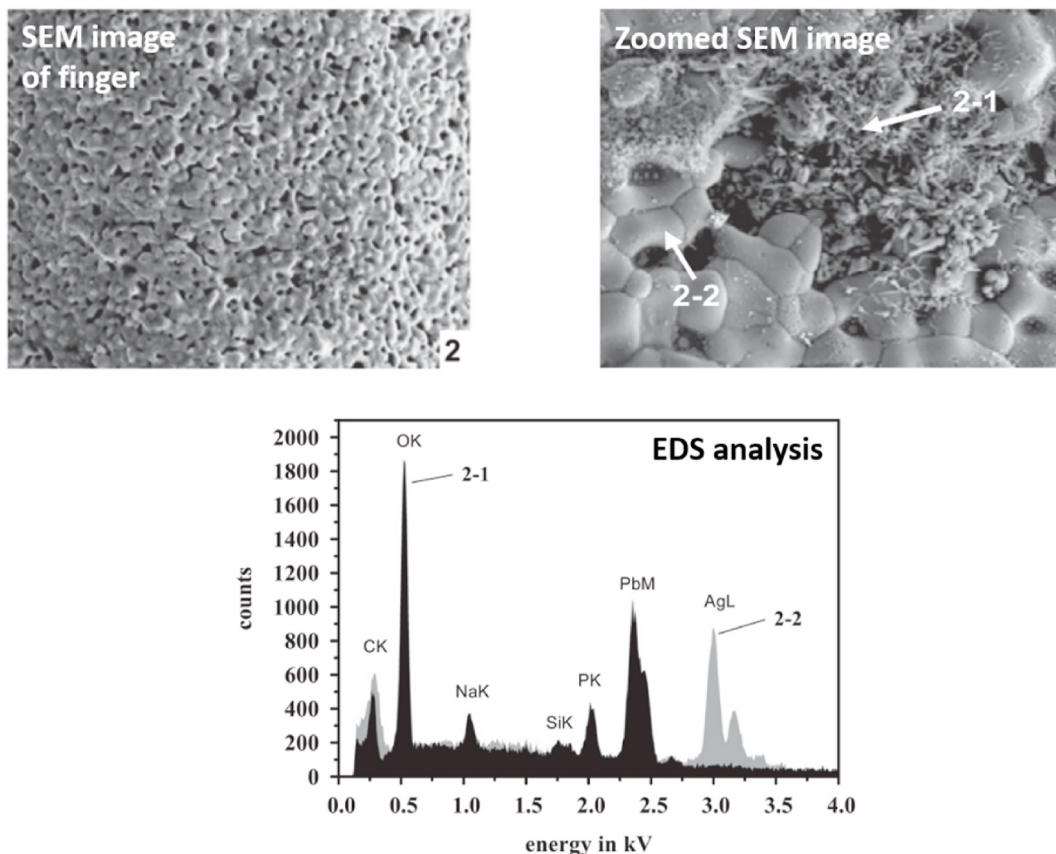


Fig. 35. SEM-EDS analysis of tin whisker formation on finger [119].

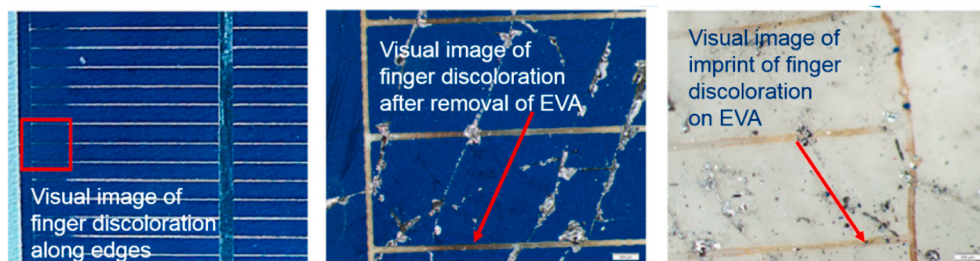


Fig. 36. Visual images of finger discolouration at cell edges, and imprints of the fingers on EVA after separation [51].

3.4.2. Interconnect burnouts

Burnouts at interconnects have often been reported in the outdoor installed modules [56,150]. An example of burnout at interconnects is shown in Fig. 40. These burnouts can be caused due to arcing faults induced in PV modules and arrays, owing to discontinuity in any current carrying conductor due to interconnector breakages and corrosion, solder joint failures etc. [151]. Arcing related failures have been reported in the outdoor field, and even led to the recalling of modules from the field [152].

It has been reported that even a 5 μm separation of interconnect ribbon with the busbar can have a dielectric breakdown due to module voltage, which produces an electric arc [153]. Such arcs have been reported to produce enough heat to shatter the glass or burn off the metal coating. Losses due to arc failures have been modelled as an R_{series} , and lead to decrease in FF. Also, mismatch losses have been observed in string connected modules [154]. Such failures can also lead to catastrophic failures leading to fires in PV modules and arrays [155]. The causes, effects of all the reviewed D & D, with the used detections and characterization techniques have been summarized in Table 1. The

summary has been divided on the basis of operating mechanisms.

4. Discussion and analysis

The recent developments in the field of advanced metallization in PV cells using different deposition and patterning techniques, and novel material development are underway. Similarly, different technologies and patterns of interconnection are being developed currently. However, the conventional and traditional forms of screen printing and soldered interconnection remain the most commonly used, due to their commercial viability. The precautions performed during the manufacturing processes including screen printing process, and interconnection process form the key to ensure a reliable performance of these metallization and interconnects. Various factors are important that either cause defects during these process, or while in outdoor field. In case of screen printing process, inadequacies in printing, improper silver paste chemical compositions and rheology, and the design parameter of the mesh need to be taken care of, to prevent finger and busbar defects. Whereas, in the interconnection process, two important steps can lead to

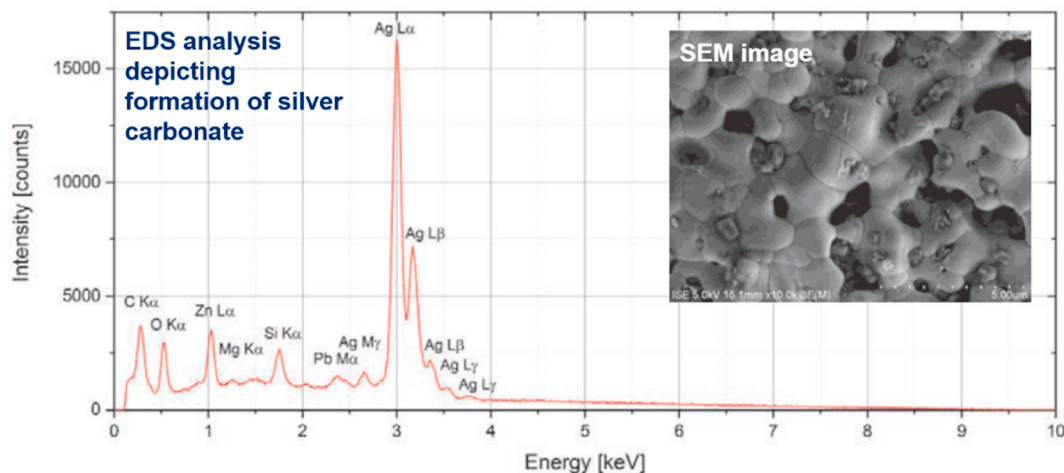


Fig. 37. EDS analysis of snail trail affected finger, depicting presence of silver carbonate as a degradation product [138].

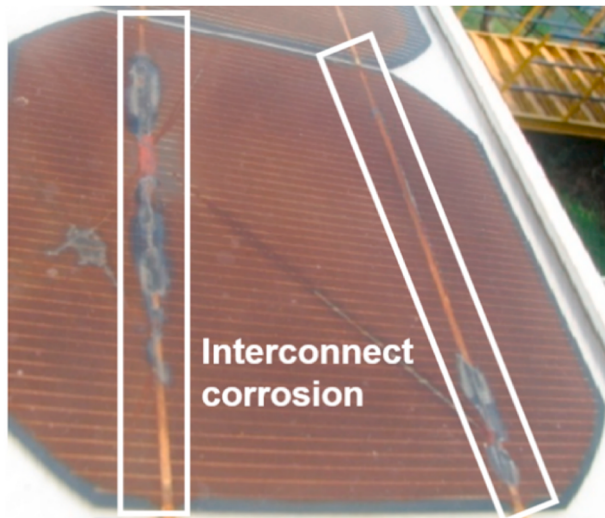


Fig. 38. Visual image of interconnect corrosion at an outdoor site [56].

defects viz. soldering process and tabbing process. Herein, the soldering process is especially crucial, and is often the breeding ground for other defects like finger breakages, IMC cracks, interconnect breakages, solder joint breakages, interconnect warpages, and tin-lead migration leading to current disruption at fingers and interconnects. This is predominantly due to the vulnerability of solder layer to thermal variation as well as moisture intrusive conditions. Even though there is extensive ongoing research on use of solder free ribbons via shingling technology for cell interconnection, which provides lower ohmic losses and lesser operating temperature, in comparison to the conventional form of soldered interconnection. However, it has various technological, as well scaling up challenges, which discourages its wide scale commercialisation. Henceforth, the conventional form of interconnection remains the primary choice, and research on enhancement of properties of solder material, and improvement of soldering process needs to be encouraged.

Structural degradation like breakages, interruptions and cracks are the dominant type of defects observed in finger metallization. These are generally induced via manufacturing fallacies and thermal transient variations in the outdoor conditions. For a wholesome review on these type of defects, the electrical impact has been simulated using PSpice circuit simulator [168]. The nuances have been investigated for change in position, number, and orientation of these defects. The schematic for finger interruptions and breakages is shown in Fig. 41 (a). Three

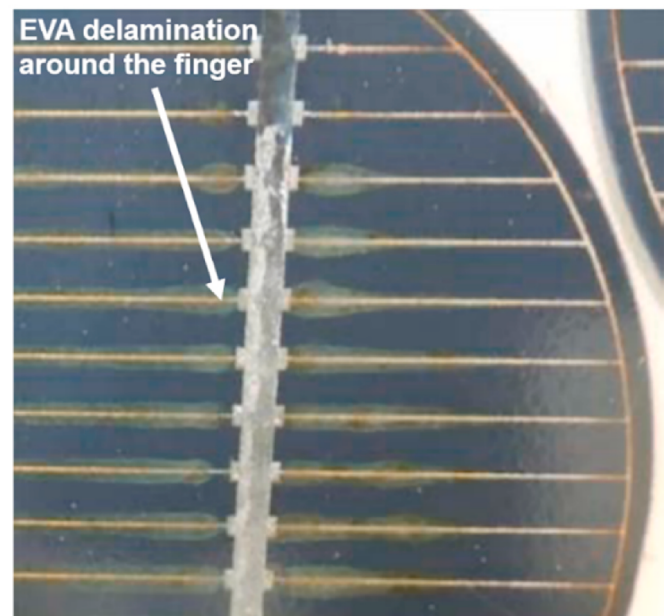


Fig. 39. Visual image of a cell with EVA delamination around the fingers [145].

positions along the finger have been taken as L1, L2, and L3, wherein, L3 represents the case of finger breakage by the solder interface. L4 represents breakages at both sides of the busbar junction, and L5-L7 represents interruptions at right hand side (or left hand side) of the busbar. The loss in P_{out} in respect of the intact finger system has been shown in Fig. 41 (b), with variation in position of interruption i.e. L1-L4 (width fixed at 1 mm), while successively increasing the number of defected fingers from 1 to 5.

The amount of loss in P_{out} in case of location L2 is observed to be slightly more than L1, which was supported by an increase in R_{series} between the two cases. This indicates that the loss in symmetry of distribution of current causes higher R_{series} , owing to increased path length in case of L2. The P_{out} losses are seen to increase as the position of interruption or breakage moves towards the busbar, wherein the case of finger breakage by the edge showed maximum P_{out} loss. However, the magnitude of these losses is significantly low in comparison to the case of dual breakage of type L4, at both ends of the busbar, which essentially renders the complete finger inactive. These demonstrated sensitivities of

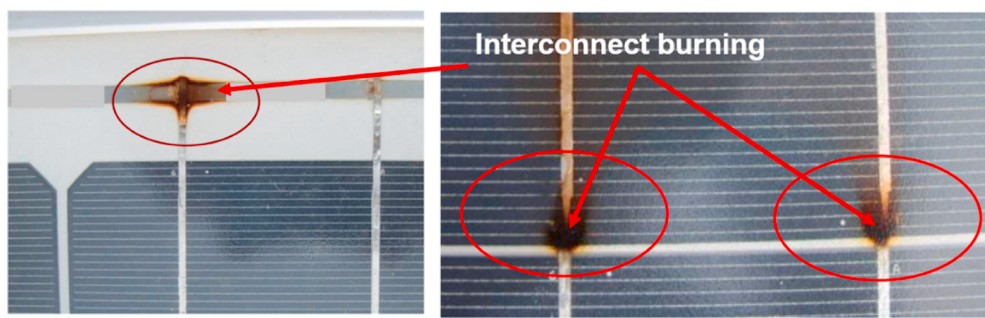


Fig. 40. Visual image of interconnect burning spots in modules installed in outdoor field [153].

Table 1

Summary of the causes and effects of finger and interconnect defects and degradations, with the used detections and characterization techniques.

Mode of degradation: Manufacturing process induced				
Defect and degradation	Finger interruptions	Finger cracks	Finger shunts	Interconnect warpage
Cause Design (de), Environmental (e), Material (ma), Manufacturing fallacy (m)	<ul style="list-style-type: none"> Insufficient paste deposition^m Damage due to external impact^m 	<ul style="list-style-type: none"> Cracks in silicon wafer^{e,m} Under accelerated test conditions: Thermal cycling test under IEC 61215 standard 	<ul style="list-style-type: none"> Deep scratches or crack in silicon wafer^{m,ma} Improper metallization contact^{de,m} Missing emitter layer during screen-printing process^m 	<ul style="list-style-type: none"> Improper tabbing process^m High coefficient of thermal expansion (CTE) of copper ribbon^{ma} Difference in CTE between cell, solder, and copper ribbon^{de,e,m,ma}
Effects Direct (d) and Indirect effects (i)	<ul style="list-style-type: none"> Restricts the flow and collection of current, due to geometrical variation in finger length which causes loss in P_{out}^d Facilitates flow of current through emitter in absence of fingers, leading to increase in R_{series} causing loss in P_{out}^i 	<ul style="list-style-type: none"> Facilitates moisture and gas ingress through backsheet, which can lead to metallization corrosion^d Can breed delamination around itself, which reduces transmission of incident radiationⁱ 	<ul style="list-style-type: none"> Leads to low shunt resistance value, which decreases open circuit voltage, leading to loss in P_{out}^d Can cause hotspot formation under reverse biasing conditionsⁱ 	<ul style="list-style-type: none"> Leads to shrinkage of ribbon-solder assembly^d Can facilitate moisture and gas ingress, which can lead to corrosion of interconnect assemblyⁱ Can facilitate accumulation of strain leading to wafer and interconnect breakages^d
Characterization techniques used for detection and analysis	EL [69] and PL imaging [78]	Visual inspection, microscopic imaging, optical inspection [21], and EL imaging [72,87,156]	EL imaging [76], EBIC, SEM-EDS, TEM [74] and DLIT [37][157,158]	EL imaging [82]
Mode of degradation: Thermo-mechanical fatigue induced				
Defect and Degradation	Finger breakage from solder-finger interface	Solder joint breakage	Intermetallic compound (IMC) cracks	Interconnect breakages
Cause Design (de), Environmental (e), Material (ma), Manufacturing fallacy (m)	<ul style="list-style-type: none"> Under transient temperature conditions^e Existing solder-joint degradations/fallacies^m Under accelerated test conditions: Thermal cycling test and humidity freeze under IEC 61215 standard 	<ul style="list-style-type: none"> Deformation under thermally stressed conditions^{m,ma} Improper soldering process^m Thermal ageing of solder material^{m,e} Under accelerated test conditions: Thermal cycling test and humidity freeze under IEC 61215 standard 	<ul style="list-style-type: none"> Tin based solder materials^{ma} Chemical reaction between tin, silver busbar, and copper ribbon^{e,ma,de} Elevated soldering temperature^m Under accelerated test conditions: Thermal cycling test under IEC 61215 standard 	<ul style="list-style-type: none"> Poor soldering at interconnect interfaces^m Improper tabbing process^m Difference in coefficient of thermal expansion of solder joint interconnect with wafer^{de,e,ma,m} Under accelerated test conditions: Thermal cycling test and humidity freeze under IEC 61215 standard Under accelerated test conditions: Thermal cycling test and humidity freeze under IEC 61215 standard
Effects Direct (d) and Indirect effects (i)	<ul style="list-style-type: none"> Disrupts the current collection by busbar, due to disruption at the busbar-finger interface, which leads to increase in R_{series}, causing loss in P_{out}^d 	<ul style="list-style-type: none"> Can lead to finger and interconnect breakages^d Causes displacement of solder material, which can provide path for moisture and gas ingress, causing metallization corrosionⁱ Causes weakening of interfacial bonds, which increases R_{series} leading to loss in P_{out}^i 	<ul style="list-style-type: none"> Leads to weakening of metallization adhesion bonds, which increases the contact resistance leading to P_{out} loss^d Facilitates moisture and gas intrusion leading to corrosion of interconnect assemblyⁱ 	<ul style="list-style-type: none"> Leads to interruption in current conduction between different cells^d Can lead to loss of adhesion with busbar, which can affect the current conduction in moduleⁱ Can lead to hot spot formation in severe casesⁱ Can cause mismatch losses in PV stringsⁱ
Characterization techniques used for detection and analysis	EL imaging [84,111,159,160], IR imaging, Visual inspection [45], and SEM-EDS [161]	SEM-EDX [65,102] and EL imaging [95]	Microscopic imaging like SEM-EDS [109,162–164], EPMA [100,105] etc.	EL imaging [82], SEM-EDS [81], Visual inspection, and IR imaging [8]
Mode of degradation: System voltage induced				
Defect and degradation	PID assisted delamination at fingers	Interconnect burnouts		
	<ul style="list-style-type: none"> High temperature and high humidity under voltage stress conditions^e 		<ul style="list-style-type: none"> Discontinuity in conductor due to interconnect breakage or corrosion^{m,e} 	

(continued on next page)

Table 1 (continued)

Mode of degradation: System voltage induced					
Defect and degradation	PID assisted delamination at fingers		Interconnect burnouts		
Cause Design (de), Environmental (e), Material (ma), Manufacturing fallacy (m)	<ul style="list-style-type: none"> Accumulation of sodium ions near busbar under the influence of voltage^e Under accelerated test conditions: PID test procedures under IEC 62804-1 standard 			<ul style="list-style-type: none"> Roller process assembly of the modules^m Arcing faults under high voltage^e 	
Effects Direct (d) and Indirect effects (i)	<ul style="list-style-type: none"> Causes loss in transmission of incident radiation^d Leads to increase in moisture and gas ingestion, which can cause metallization corrosionⁱ 			<ul style="list-style-type: none"> Leads to dramatic change in material chemical composition, causing very high R_{series}, resulting in significant P_{out} loss^d Can cause mismatch losses in PV module stringsⁱ Can cause hotspots induced backsheet burn and broken glassⁱ Can cause catastrophic fires in PV fieldsⁱ 	
Characterization techniques used for detection and analysis	ToF-SIMS, SEM-EDS, EBIC, DLIT, EL [146,167], and visual inspection[145] [147]			Visual inspection [11,150,152]	
Mode of degradation: Chemical induced degradation					
Defect and degradation	Silver oxide deposition on fingers	Snail trails	Glass frit corrosion and finger delamination	Solder material degradation	Interconnect corrosion
Cause Design (de), Environmental (e), Material (ma), Manufacturing fallacy (m)	<ul style="list-style-type: none"> High temperature with high humidity conditions^e Lateral diffusion of gases and moisture over cell from edges^{d,e} Diffusion path for moisture and gases through pre-existing cracks^{e,m} Under accelerated test conditions: Damp heat test and humidity freeze test under IEC 61215 standard 	<ul style="list-style-type: none"> Pre-existing micro-cracks^m Ingression of moisture and gases through cracks^{e,m} Formation of nanoparticles on silver finger due to reaction with encapsulant material^{e,ma} Under accelerated test conditions: Damp heat test under IEC 61215 standard 	<ul style="list-style-type: none"> Dependent on the glass phase composition in silver paste^{ma} Moisture and gases, like CO_2 promotes corrosion of silica glass grit^e Acetic acid formed during discoloration of EVA^{e,ma} Under accelerated test conditions: Damp heat test under IEC 61215 standard 	<ul style="list-style-type: none"> Moisture and gases ingress under high temperature^e Low oxidation potential of causing preferential galvanic corrosion of solder material^{ma,e} Under accelerated test conditions: Damp heat test under IEC 61215 standard 	<ul style="list-style-type: none"> high temperature^{e,ma} Preferential galvanic corrosion of solder material caused void, promotes moisture and gas intrusion^{e,ma} Migration of aluminium, and solder material as oxides, at the rear of the interconnect ribbon^e Acetic acid released during discoloration of EVA^{e,ma} Under accelerated test conditions: Damp heat test under IEC 61215 standard
Effects Direct (d) and Indirect effects (i)	<ul style="list-style-type: none"> Reduces cross-sectional area of finger, causing increase in local R_{series}, leading to P_{out} loss^d Cause change in material composition, which affects the metallization conductivityⁱ 	<ul style="list-style-type: none"> Leads to formation of silver compounds, which can affect material conductivity, causing loss in P_{out}^d Leads to delamination along itself, which can cause metallization corrosion and reduction of incident light transmission^d 	<ul style="list-style-type: none"> Leads to loss in contact between emitter and metallization, causing increase in contact resistance^d Causes changes in chemical composition of glass grits Can facilitate moisture and gases ingress, leading to metallization corrosionⁱ 	<ul style="list-style-type: none"> Leads to displacement of solder material, which affects the current collection at busbar^d Can cause adhesion loss between interconnect ribbon and busbar, increasing contact resistanceⁱ 	<ul style="list-style-type: none"> Leads to oxide formation at the rear of copper ribbon, reducing its conductivity, causing P_{out} loss^d Causes loss of adhesion between interconnect and busbar, thereby increasing contact resistanceⁱ Causes appearance of yellow and green coating over ribbonⁱ Can cause hot spots in severe casesⁱ
Characterization techniques used for detection and analysis	Visual inspection [33], SEM-EDS, EL imaging, DLIT, and AES [39,50,120]	Visual inspection, SEM-EDS, TEM, EL imaging, ToF-SIMS [51, 139], XPS [165], IR thermography, Raman spectroscopy [138,142], Fluorescence radiation and FTIR [134]	I-V characteristics, AC impedance signal [125], SEM-EDS, , Chemical trace analysis, XRD [49,130], and Cyclic voltammetry [124]	IQE [119], SEM-EDS, EL imaging, and AES [39, 50,120,131,132,166]	Visual inspection, IR imaging [11,121], EL imaging, SEM-EDS [39, 112], and XPS [144]

the electrical loss to position and amount of breakages, and indicates the need to exercise the precautions in terms of printing process and setting of design parameters.

The cell to cell cracks also lead to finger and busbar breakages. There are multiple factors which will determine the impact of electrical loss due to cell to cell cracks. Herein, the loss in P_{out} can be associated with two types of modes of electrical loss viz. R_{series} effects and generation loss. For the purpose of understanding, different cases of wafer cracks affecting metallization have been simulated as shown in Fig. 42 (a). The corresponding loss in the electrical parameters has been shown in Fig. 42 (b). In case of type A, the symmetry of current conduction is not much interrupted causing current from emitter to flow through intact fingers,

leading to low resistive losses. While moving towards the busbar (type B) there is a slight increase in loss in R_{series} owing to the extra path to be travelled by current due to loss in symmetry. Thereby, indicating the severity of position of cell to cell crack in respect of symmetry of current distribution. The position of crack in respect of busbar is also crucial. In case of type C, even though the busbar remains unbroken, the position of crack completely isolates around one-third portion of cell, causing loss in current generation, which is reflected in loss in short circuit current for type C. Furthermore, the type of rear side busbar tabbing of ribbon viz. full over the complete busbar or partial at the cell edges, is a major factor which determines the severity of different orientations of cell to cell cracks. The case of type D has been simulated for the case of full

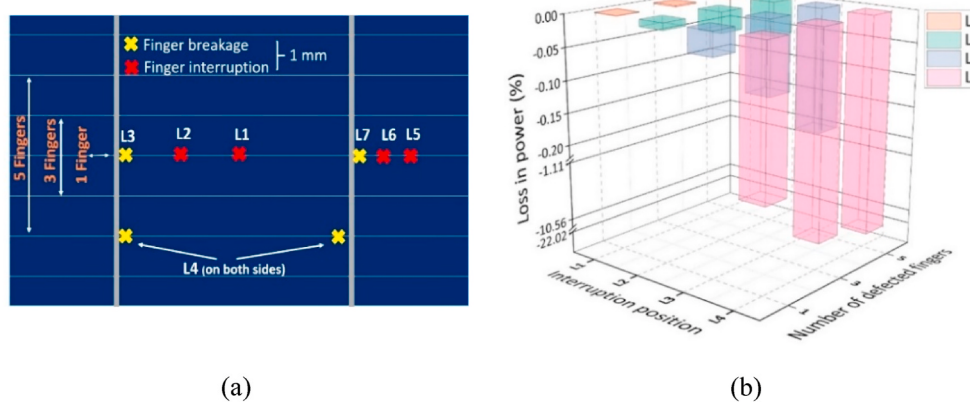


Fig. 41. (a) Illustration of simulated finger interruptions and breakages (b) Loss in P_{out} with change in position and number of defected fingers.

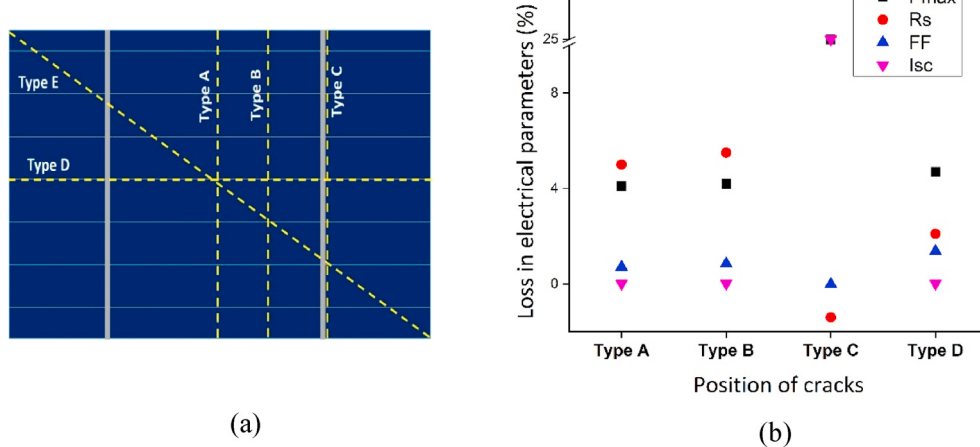


Fig. 42. (a) Illustration of simulated cases of cracks (b) Loss in electrical parameters for different cases of cell to cell cracks.

tabbing, wherein, significantly less P_{out} loss is observed in comparison to the type C case. Herein, the copper ribbon remains intact even in presence of a cracked busbar, thereby ensuring the integrity of the circuit, even though there would be some resistive losses. Such losses will be very severe in case of half tabbing wherein, the other part of cell (which is not in contact with the busbar) will be ineffective. Hence, the tabbing of ribbon at rear of cell, is a crucial parameter for determining the severity of losses due to such cracks.

The chemically induced degradation is the second most commonly observed metallization and interconnect degradation. The susceptibility of backsheet and encapsulant packaging in PV modules to moisture and gas ingressions forms the main reason for such type of degradation. The DH test conditions are found to be well replicating, of such defects which are observed in the external field conditions, by accelerated simulation of moisture and gases transmission. In contrast to the commonly used term corrosion for all types of chemical degradation, different degradation products have been reported for both metallization and interconnects, under similar moisture and gases ingestion. However, migration of solder alloy materials on fingers and interconnects has been identified to be the more common mode of chemical degradation. Also, the loss in P_{out} in case of tin-lead migration, has been reported to be more than the other cases of localised compound formation on finger and interconnects. These chemical degradation products have dissimilar modes of electrical loss, irrespective of the final effect on R_{series} . The details of these effects for each reviewed chemical degradation has been provided in Table 1. These degradation products affect the current flow in the cell, either by disruption due to formation of non-conductive

material or physical obstruction due to migration of material components. The understanding of these dissimilar modes has been used for quick identification and differentiation by signature imaging patterns, for few cases of chemical degradation. The effective use of imaging techniques for other chemical degradation is also recommended, to avoid any destructive analysis of the modules. Furthermore, some chemical degradations like snail trail and yellow coating on ribbons do not much affect the electrical performance of cells and modules, despite formation of new chemical compounds. Thereby, research can be directed towards comparison of severity of different defects, which would help in defect prioritisation for mitigation.

5. Conclusions

This paper covered a detailed review and analysis on the defects and degradation in crystalline silicon photovoltaic (PV) cell metallization and interconnects. The reliability of operation of these current carrying components is quintessential to the performance of PV modules. However, they are prone to defects and degradation causing disruption in current conduction and collection, where losses are palpable as instantaneous performance loss, and can lead to long term failures in the outdoor installed field modules. Such defects and degradations are prominently caused due to manufacturing fallacies, environmental conditions, and existing defects. The broad findings and suggestions from this review are as follows:

- These particular cell components are, especially vulnerable in regions with large variations in day and night temperature (like deserts), or those with hot and humid climatic conditions. Thereby, relevant defect specific pre-testing of PV module batches needs to be conducted before their installation.
- The structural degradation like breakages, interruptions and cracks are the dominant type of defects observed in fingers metallization. Whereas, multiple forms of chemically induced degradation is the second most commonly observed in fingers and interconnects.
- Standard tests defined under IEC 61215 qualification testing viz. thermal cycling tests and damp heat test are instrumental in observing metallization and interconnect defects in lab environment. However, it is to be kept in mind that these qualifications tests do not ensure reliable long term operation standard, hence, defect specific tests may be devised, to simulate the occurrence of these defects for an in-depth analysis.
- The defects in metallization and interconnects are generally not visible to the naked eye. Hence, use of imaging techniques should be further exploited, for use in the manufacturing stage as well as outdoor field. The effective use of these commonly used characterization techniques is an essential aspect for understanding, as well as detection and mitigation of these defects.
- The electrical impact of the defects was found to be sensitive to change in position, number, and orientation of the finger defects.
- The manufacturing processes including screen printing process, and interconnection process form the key to ensure a reliable performance of these metallization and interconnects. Proper precautions should be performed especially during the tabbing, soldering and screen printing process.

CRediT authorship contribution statement

Sagarika Kumar: Conceptualization, Methodology, Investigation, Formal analysis, Writing – original draft, Visualization. **Roopmati Meena:** Formal analysis, Investigation, Writing – review & editing. **Rajesh Gupta:** Supervision, Resources, Project administration, Writing – review & editing.

Declaration of competing interest

The authors declare that they have no known competing financial interests or personal relationships that could have appeared to influence the work reported in this paper.

Acknowledgement

The authors would like to thank Dr. Manish Kumar from Indian Institute of Technology Bombay, India for providing valuable suggestions for preparation of the manuscript.

References

- [1] I. Fraunhofer, Photovoltaics Report, 2019.
- [2] International Energy Agency, Assessment of PV Module Failures in the Field, 2017.
- [3] M.T. Zarmai, N.N. Ekere, C.F. Oduoza, E.H. Amalu, A review of interconnection technologies for improved crystalline silicon solar cell photovoltaic module assembly, *Appl. Energy* 154 (2015) 173–182, <https://doi.org/10.1016/j.apenergy.2015.04.120>.
- [4] A.A.B. Baloch, S. Hammam, B. Figgis, F.H. Alharbi, N. Tabet, In-field characterization of key performance parameters for bifacial photovoltaic installation in a desert climate, *Renew. Energy* 159 (2020) 50–63, <https://doi.org/10.1016/j.renene.2020.05.174>.
- [5] J. Libal, R. Kopecek, Bifacial Photovoltaics: Technology, Applications and Economics, 2018, <https://doi.org/10.1049/pbpo107e>.
- [6] F. Haase, C. Hollemann, S. Schäfer, A. Merkle, M. Rienäcker, J. Krügner, et al., Laser contact openings for local poly-Si-metal contacts enabling 26.1%-efficient POLO-IBC solar cells, *Sol. Energy Mater. Sol. Cells* 186 (2018) 184–193, <https://doi.org/10.1016/j.solmat.2018.06.020>.
- [7] A. Blakers, Development of the PERC solar cell, *IEEE J Photovoltaics* 9 (2019) 629–635, <https://doi.org/10.1109/JPHOTOV.2019.2899460>.
- [8] V. Sharma, S.S. Chandel, A novel study for determining early life degradation of multi-crystalline-silicon photovoltaic modules observed in western Himalayan Indian climatic conditions, *Sol. Energy* 134 (2016) 32–44, <https://doi.org/10.1016/j.solener.2016.04.023>.
- [9] P. Hülsmann, K.A. Weiss, Simulation of water ingress into PV-modules: IEC-testing versus outdoor exposure, *Sol. Energy* 115 (2015) 347–353, <https://doi.org/10.1016/j.solener.2015.03.007>.
- [10] M. Kumar, A. Kumar, Performance assessment and degradation analysis of solar photovoltaic technologies: a review, *Renew. Sustain. Energy Rev.* 78 (2017) 554–587, <https://doi.org/10.1016/j.rser.2017.04.083>.
- [11] P. Rajput, G.N. Tiwari, O.S. Sastry, B. Bora, V. Sharma, Degradation of monocrystalline photovoltaic modules after 22 years of outdoor exposure in the composite climate of India, *Sol. Energy* 135 (2016) 786–795, <https://doi.org/10.1016/j.solener.2016.06.047>.
- [12] M.A. Quintana, D.L. King, T.J. McMahon, C.R. Osterwald, Commonly Observed Degradation in Field-Aged Photovoltaic Modules, 2003, pp. 1436–1439, <https://doi.org/10.1109/pvsc.2002.1190879>.
- [13] Chatterpadhyay RD, Shashwata, Shashwata Chatterpadhyay, Rajiv Dubey, Vivek Kuthanazhi, Sachin Zachariah, C.M. Sonali Bhaduri, Sugguna Rambabu, Firoz Ansari, Amey Chindarkar, Archana Sinha, Hemant Kumar Singh, Narendra Shiradkar, Brij Mohan Arora, Anil Kottantharayil, K. L, S. S. Narasimhan, JV, All-India Survey of Photovoltaic Module Reliability: 2016 All-India Survey of Photovoltaic Module Reliability: 2016, 2017, p. 217.
- [14] N.G. Dhere, N.R. Ravavikar, A. Mikonowicz, C. Cording, Effect of glass Na content on adhesional strength of PV modules, in: Conf Rec IEEE Photovolt Spec Conf, 2002, <https://doi.org/10.1109/pvsc.2002.1190498>, 231–4.
- [15] D. Quansah, M. Adaramola, G. Takyi, I. Edwin, Reliability and degradation of solar PV modules—case study of 19-year-old polycrystalline modules in Ghana, *Technologies* 5 (2017) 22, <https://doi.org/10.3390/technologies5020022>.
- [16] P. Sanchez-Friera, M. Piliouugine, J. Pelaez, J. Carretero, MS De Cardona, Analysis of degradation mechanisms of crystalline silicon PV modules after 12 years of operation in Southern Europe, *Prog. Photovoltaics Res. Appl.* 19 (2011) 658–666, <https://doi.org/10.1002/pip>.
- [17] J.M. Kuitche, G. Tamizh-Mani, R. Pan, Failure modes effects and criticality analysis (FMEA) approach to the crystalline silicon photovoltaic module reliability assessment, *Reliab. Photovoltaic Cells, Modul Components, Syst IV* 8112 (2011) 81120L, <https://doi.org/10.1117/12.894301>.
- [18] K. Yedidi, S. Tatapudi, J. Mallineni, B. Knisely, J. Kutiche, G. Tamizhmani, Failure and degradation modes and rates of PV modules in a hot-dry climate: results after 16 years of field exposure, in: 2014 IEEE 40th Photovolt Spec Conf PVSC 2014, 2014, <https://doi.org/10.1109/PVSC.2014.6925626>, 3245–7.
- [19] B. Bora, O.S. Sastry, R. Kumar, R. Dubey, S. Chatterpadhyay, J. Vasi, et al., Failure mode analysis of PV modules in different climatic conditions, *IEEE J Photovoltaics* 11 (2021) 453–460, <https://doi.org/10.1109/JPHOTOV.2020.3043847>.
- [20] MCC de Oliveira, A.S.A. Diniz Cardoso, M.M. Viana, V. de FC. Lins, The causes and effects of degradation of encapsulant ethylene vinyl acetate copolymer (EVA) in crystalline silicon photovoltaic modules: a review, *Renew. Sustain. Energy Rev.* 81 (2018) 2299–2317, <https://doi.org/10.1016/j.rser.2017.06.039>.
- [21] L. Papargyri, M. Theristis, B. Kubicek, T. Krametz, C. Mayr, P. Papanastasiou, et al., Modelling and experimental investigations of microcracks in crystalline silicon photovoltaics: a review, *Renew. Energy* 145 (2020) 2387–2408, <https://doi.org/10.1016/j.renene.2019.07.138>.
- [22] A. Omazic, G. Oreski, M. Halwachs, G.C. Eder, C. Hirschl, L. Neumaier, et al., Relation between degradation of polymeric components in crystalline silicon PV module and climatic conditions: a literature review, *Sol. Energy Mater. Sol. Cells* 192 (2019) 123–133, <https://doi.org/10.1016/j.solmat.2018.12.027>.
- [23] H. Mohammed, R. Gupta, O. Sastry, D. Magare, Assessment of different correlations to estimate distinct technology PV module operating temperature for Indian site, *Energy Sci Eng* 4–7 (2019), <https://doi.org/10.1002/ese3.332>.
- [24] A. Ndiaye, C.M.F. Kébé, A. Charaki, P.A. Ndiaye, V. Sambou, A. Kobi, Degradation evaluation of crystalline-silicon photovoltaic modules after a few operation years in a tropical environment, *Sol. Energy* 103 (2014) 70–77, <https://doi.org/10.1016/j.solener.2014.02.006>.
- [25] A. Ndiaye, A. Charaki, A. Kobi, A CMF. Kébé, P.A. Ndiaye, V. Sambou, Degradations of silicon photovoltaic modules: a literature review, *Sol. Energy* 96 (2013) 140–151, <https://doi.org/10.1016/j.solener.2013.07.005>.
- [26] A. Bouraïou, M. Hamouda, A. Chaker, A. Nécaibia, M. Mostefoui, N. Boutasseta, et al., Experimental investigation of observed defects in crystalline silicon PV modules under outdoor hot dry climatic conditions in Algeria, *Sol. Energy* 159 (2018) 475–487, <https://doi.org/10.1016/j.solener.2017.11.018>.
- [27] S. Goranti, G. Tamizhmani, Potential induced degradation (PID) study on accelerated stress tested PV modules, in: Conf Rec IEEE Photovolt Spec Conf, 2012, pp. 2438–2441, <https://doi.org/10.1109/PVSC.2012.6318088>.
- [28] N.C. Park, W.W. Oh, D.H. Kim, Effect of temperature and humidity on the degradation rate of multicrystalline silicon photovoltaic module, *Int. J. Photoenergy* 2013 (2013) 1–9, <https://doi.org/10.1155/2013/925280>.
- [29] L.N. Dumas, A. Shumka, Photovoltaic module reliability improvement through application testing and failure analysis, *IEEE Trans. Reliab.* R-31 (1982) 228–234, <https://doi.org/10.1109/TR.1982.5221325>.
- [30] T.J. McMahon, Accelerated testing and failure of thin-film PV modules, *Prog. Photovoltaics Res. Appl.* 12 (2004) 235–248, <https://doi.org/10.1002/pip.526>.
- [31] M. Koehl, M. Heck, S. Wiesmeier, Modelling of conditions for accelerated lifetime testing of Humidity impact on PV-modules based on monitoring of climatic data,

- Sol. Energy Mater. Sol. Cells 99 (2012) 282–291, <https://doi.org/10.1016/j.solmat.2011.12.011>.
- [32] J.H. Wohlgemuth, D.W. Cunningham, P. Monus, J. Miller, A. Nguyen, Long term reliability of photovoltaic modules, in: Conf Rec 2006 IEEE 4th World Conf Photovolt Energy Conversion, WCPEC-4 vol. 2, 2006, <https://doi.org/10.1109/WCPEC.2006.279905>, 2050–3.
- [33] E.E. Van Dyk, J.B. Chamel, A.R. Gxasheka, Investigation of delamination in an edge-defined film-fed growth photovoltaic module, Sol. Energy Mater. Sol. Cells 88 (2005) 403–411, <https://doi.org/10.1016/j.solmat.2004.12.004>.
- [34] R. Meena, S. Kumar, R. Gupta, Comparative investigation and analysis of delaminated and discolored encapsulant degradation in crystalline silicon photovoltaic modules, Sol. Energy 203 (2020) 114–122, <https://doi.org/10.1016/j.solener.2020.04.041>.
- [35] M.F. Stuckings, A.W. Blakers, A study of shading and resistive loss from the fingers of encapsulated solar cells, Sol. Energy Mater. Sol. Cells 59 (1999) 233–242.
- [36] R. De Rose, A. Malomo, P. Magnone, F. Crupi, G. Cellere, M. Martire, et al., A methodology to account for the finger interruptions in solar cell performance, Microelectron. Reliab. 52 (2012) 2500–2503, <https://doi.org/10.1016/j.micrel.2012.07.014>.
- [37] S. Roy, R. Gupta, Non-destructive approach for severity investigation of shunts in crystalline silicon photovoltaic modules by combination of electroluminescence imaging and lock-in thermography, Meas. Sci. Technol. 30 (2019), 044009, <https://doi.org/10.1088/1361-6501/ab0265>.
- [38] C. Yüce, K. Okamoto, L. Karpowich, A. Adrian, N. Willenbacher, Non-volatile free silver paste formulation for front-side metallization of silicon solar cells, Sol. Energy Mater. Sol. Cells 200 (2019) 110040, <https://doi.org/10.1016/j.solmat.2019.110040>.
- [39] S. Kumar, R. Meena, R. Gupta, Imaging and micro-structural characterization of moisture induced degradation in crystalline silicon photovoltaic modules, Sol. Energy 194 (2019) 903–912, <https://doi.org/10.1016/j.solener.2019.11.037>.
- [40] A. Eslami Mjad, N.N. Ekere, Numerical analysis on thermal crack initiation due to non-homogeneous solder coating on the round strip interconnection of photovoltaic modules, Sol. Energy 194 (2019) 649–655, <https://doi.org/10.1016/j.solener.2019.10.092>.
- [41] IEC 61215, IEC-61215, Crystalline Silicon Terrestrial Photovoltaic (PV) Modules-Design, Qualification and Type Approval, 2005.
- [42] IEC-61215-1, Terrestrial Photovoltaic (PV) Modules-Design Qualification and Type Approval-Part 1-1: Special Requirement for Testing of Crystalline Silicon Photovoltaic (PV) Mdoules, 2016.
- [43] R. Chen, W. Zhang, X. Wang, X. Wang, A. Lennon, Failure modes identified during adhesion testing of metal fingers on silicon solar cells, Energy Procedia 67 (2015) 194–202, <https://doi.org/10.1016/j.egypro.2015.02.087>.
- [44] A. Bouraiou, M. Hamouda, A. Chaker, A. Neçibia, M. Mostefaoui, N. Boutasseta, et al., Experimental investigation of observed defects in crystalline silicon PV modules under outdoor hot dry climatic conditions in Algeria, Sol. Energy 159 (2018) 475–487, <https://doi.org/10.1016/j.solener.2017.11.018>.
- [45] P. Chaturvedi, B. Hoex, T.M. Walsh, Broken metal fingers in silicon wafer solar cells and PV modules, Sol. Energy Mater. Sol. Cells 108 (2013) 78–81, <https://doi.org/10.1016/j.solmat.2012.09.013>.
- [46] I. Zafirovska, M. Juhl, J.W. Weber, J. Wong, T. Trupke, Detection of finger interruptions in silicon solar cells using photoluminescence imaging, IEEE J Photovoltaics 7 (2017) 1496–1502, <https://doi.org/10.1088/1674-1056/27/6/068801>.
- [47] S. Kumar, S. Roy, R. Gupta, Characterization of degradation under standard environmental testing methods for crystalline silicon photovoltaic modules, Int J Power Energy Res 1 (2017) 150–158, <https://doi.org/10.22606/ijper.2017.13002>.
- [48] A. Sinha, S. Roy, S. Kumar, R. Gupta, Investigation of degradation in photovoltaic modules by infrared and electroluminescence imaging, Springer Proc. Phys. 194 (2017) 3–9, https://doi.org/10.1007/978-981-10-3908-9_1.
- [49] T. Semba, T. Shimada, K.Y.K. Shirasawa, H. Takato, Corrosion of the glass and formation of lead compounds in the metallization by high temperature and high humidity test of crystalline silicon PV module, in: 2018 IEEE 7th World Conf Photovolt Energy Conversion, WCPEC 2018 - A Jt Conf 45th IEEE PVSC, 28th PVSEC 34th EU PVSEC, 2018, <https://doi.org/10.1109/PVSC.2018.8548005>, 1333–5.
- [50] H. Xiong, C. Gan, X. Yang, Z. Hu, H. Niu, J. Li, et al., Corrosion behavior of crystalline silicon solar cells, Microelectron. Reliab. 70 (2017) 49–58, <https://doi.org/10.1016/j.micrel.2017.01.006>.
- [51] S. Meyer, S. Timmel, S. Richter, M. Werner, M. Gläser, S. Swatek, et al., Silver nanoparticles cause snail trails in photovoltaic modules, Sol. Energy Mater. Sol. Cells 121 (2014) 171–175, <https://doi.org/10.1016/j.solmat.2013.11.013>.
- [52] G.J. Jorgensen, K.M. Terwilliger, J.A. DelCueto, S.H. Glick, M.D. Kempe, J. W. Pankow, et al., Moisture transport, adhesion, and corrosion protection of PV module packaging materials, Sol. Energy Mater. Sol. Cells 90 (2006) 2739–2775, <https://doi.org/10.1016/j.solmat.2006.04.003>.
- [53] J.A. Tsanakas, L. Ha, C. Buerhop, Faults and infrared thermographic diagnosis in operating c-Si photovoltaic modules: a review of research and future challenges, Renew. Sustain. Energy Rev. 62 (2016) 695–709, <https://doi.org/10.1016/j.rser.2016.04.079>.
- [54] O.O. Ogbomo, E.H. Amalu, N.N. Ekere, P.O. Olagbegi, Effect of operating temperature on degradation of solder joints in crystalline silicon photovoltaic modules for improved reliability in hot climates, Sol. Energy 170 (2018) 682–693, <https://doi.org/10.1016/j.solener.2018.06.007>.
- [55] O.O. Ogbomo, E.H. Amalu, N.N. Ekere, P.O. Olagbegi, Effect of coefficient of thermal expansion (CTE) mismatch of solder joint materials in photovoltaic (PV) modules operating in elevated temperature climate on the joint's damage, Procedia Manuf 11 (2017) 1145–1152, <https://doi.org/10.1016/j.promfg.2017.07.236>.
- [56] Rajiv Dubey, V.K. Shashwata Chattopadhyay, Jim Joseph John, B.M. Arora, Anil Kottantharayil, K.L. Narasimhan, Chetan S. Solanki, Vaman Kuber, A. K. Juizer Vasi, OSSS, All-India India Survey of Photovoltaic Module Degradation: 2013, 2013.
- [57] P. Rajput, G.N. Tiwari, O.S. Sastry, Thermal modelling and experimental validation of hot spot in crystalline silicon photovoltaic modules for real outdoor condition, Sol. Energy 139 (2016) 569–580, <https://doi.org/10.1016/j.solener.2016.10.016>.
- [58] A. Lorenz, C. Gredy, M. Lehner, R. Greutmann, H. Brocker, J. Rohde, et al., Progress with Rotational Printing for the Front Side Metallization of Silicon Solar Cells, EUPVSEC, 2016, pp. 413–419, <https://doi.org/10.4229/EUPVSEC20162016-2CO.2.4>.
- [59] P. Magnone, G. Napoletano, R. De Rose, F. Crupi, D. Tonini, G. Cellere, et al., A methodology to account for the finger non-uniformity in photovoltaic solar cell, Energy Procedia 27 (2012) 191–196, <https://doi.org/10.1016/j.egypro.2012.07.050>.
- [60] C. Honsberg, S. Bowden, PVEducation, n.d. <https://www.pveducation.org/pvcdrom/manufacturing-si-cells/screen-printed-solar-cells>. (Accessed 2 May 2020).
- [61] C. Peike, S. Hoffmann, I. Dürr, K.A. Weiß, M. Koehl, The influence of laminate design on cell degradation, Energy Procedia 38 (2013) 516–522, <https://doi.org/10.1016/j.egypro.2013.07.311>.
- [62] A. Mondon, J. Bartsch, B.J. Godejohann, M. Hörtelis, S. Glunz, Advanced front side metallization for crystalline silicon solar cells based on a nickel-silicon contact, in: 2nd Work. Met. Cryst. Silicon Sol. Cells, 2010, pp. 42–47.
- [63] J.D. Fields, M.I. Ahmad, V.L. Pool, J. Yu, D.G. Van Campen, P.A. Parilla, et al., The formation mechanism for printed silver-contacts for silicon solar cells, Nat. Commun. 7 (2016) 1–7, <https://doi.org/10.1038/ncomms11143>.
- [64] C. Yu, R. Chen, J.J. Li, J.J. Li, M. Drahansky, M. Paridah, et al., Screen-printed front junction n-type silicon solar cells, Print. Electron. Trends Appl. (2012) 29, <https://doi.org/10.5772/63198>.
- [65] J.S. Jeong, N. Park, C. Han, Field failure mechanism study of solder interconnection for crystalline silicon photovoltaic module, Microelectron. Reliab. 52 (2012) 2326–2330, <https://doi.org/10.1016/j.micrel.2012.06.027>.
- [66] M. Neidert, W. Zhang, D. Zhang, A. Kipka, Screen-printing simulation study on solar cell front side AG paste, in: Conf. Rec. IEEE Photovolt. Spec. Conf., 2008, pp. 14–17, <https://doi.org/10.1109/PVSC.2008.4922793>.
- [67] S. Kumar, R. Gupta, Thermo-mechanical degradation at finger-solder interface in a crystalline silicon photovoltaic module under thermal fatigue conditions, in: Conf. Rec. IEEE Photovolt Spec Conf, 2019, <https://doi.org/10.1109/PVSC40753.2019.8980538>, 0118–21.
- [68] S. Kumar, R. Gupta, Influence of cell packaging and design parameters on thermo-mechanical reliability of fingers in crystalline silicon photovoltaic modules, AIP Conf Proc 2147 (2019), 090002, <https://doi.org/10.1063/1.5123870>.
- [69] D.C. Tseng, Y.S. Liu, C.M. Chou, Automatic finger interruption detection in electroluminescence images of multicrystalline solar cells, Math. Probl Eng. 2015 (2015), <https://doi.org/10.1155/2015/879675>.
- [70] I. Zafirovska, M. Juhl, T. Trupke, Efficient detection of finger interruptions from photoluminescence images, in: 33th EUPVSEC, 2017, pp. 1689–1693, <https://doi.org/10.4229/EUPVSEC20172017-5BV.4.65>.
- [71] M. Paggi, I. Berardone, A. Infuso, M. Corrado, Fatigue degradation and electric recovery in Silicon solar cells embedded in photovoltaic modules, Sci. Rep. 4 (2014) 4506, <https://doi.org/10.1038/srep04506>.
- [72] I. Berardone, M. Corrado, M. Paggi, A generalized electric model for mono and polycrystalline silicon in the presence of cracks and random defects, Energy Procedia 55 (2014) 22–29, <https://doi.org/10.1016/j.egypro.2014.08.005>.
- [73] O. Breitenstein, J. Bauer, J.P. Rakotonaina, Material-induced shunts in multicrystalline silicon solar cells, Semiconductors 41 (2007) 440–443, <https://doi.org/10.1134/s106378260704015x>.
- [74] O. Breitenstein, J.P. Rakotonaina, M.H. Al Rifai, M. Werner, Shunt types in crystalline silicon solar cells, Prog. Photovoltaics Res. Appl. 12 (2004) 529–538, <https://doi.org/10.1002/pip.544>.
- [75] P. Somasundaran, R. Gupta, Influence of local shunting on the electrical performance in industrial Silicon solar cells, Sol. Energy 139 (2016) 581–590, <https://doi.org/10.1016/j.solener.2016.10.200>.
- [76] S. Roy, R. Gupta, Quantitative estimation of shunt resistance in crystalline silicon photovoltaic modules by electroluminescence imaging, IEEE J Photovoltaics 9 (2019) 1741–1747, <https://doi.org/10.1109/JPHOTOV.2019.2930402>.
- [77] O. Breitenstein, J. Bauer, K. Bothe, W. Kwapis, D. Lausch, U. Rau, et al., Understanding junction breakdown in multicrystalline solar cells, J. Appl. Phys. 109 (2011), 071101, <https://doi.org/10.1063/1.3562200>.
- [78] E.L. Meyer, E. Ernest van Dyk, The effect of reduced shunt resistance and shading on photovoltaic module performance, IEEE J Photovoltaics (2005), <https://doi.org/10.1109/pvsc.2005.1488387>, 1331–4.
- [79] M. Barbato, M. Meneghini, V. Giliberto, D. Giaffreda, P. Magnone, R. De Rose, et al., Effect of shunt resistance on the performance of mc-Silicon solar cells: a combined electro-optical and thermal investigation, in: Conf. Rec. IEEE Photovolt. Spec. Conf., 2012, pp. 1241–1245, <https://doi.org/10.1109/PVSC.2012.6317827>.

- [80] A. Halm, E. Lemp, R. Farneda, J. Theobald Rh, Method to counter warpage due to stringing for back contact solar cells, in: Eur. Photovolt. Sol. Energy Conf. Exhib., 2017, pp. 989–991, <https://doi.org/10.4229/EUPVSEC20172017-2CV.2.91>.
- [81] B. Kang, N. Park, S.J. Tark, W.W. Oh, S. Park, Y Do Kim, et al., Advanced yield strength of interconnector ribbon for photovoltaic module using crystallographic texture control, Met. Mater. Int. 20 (2014) 229–232, <https://doi.org/10.1007/s12540-014-2005-x>.
- [82] Y. Zemen, T. Prewitz, T. Geipel, S. Pingel JB, The impact of yield strength of the interconnector on the internal stress of the solar cell within a module, in: PVSEC 25th, 2010, pp. 6–10, <https://doi.org/10.4229/25thEUPVSEC2010-4AV.3.38>.
- [83] N. Bosco, T.J. Silverman, S. Kurtz, The influence of PV module materials and design on solder joint thermal fatigue durability, IEEE J Photovoltaics 6 (2016) 1407–1412.
- [84] S. Kumar, R. Gupta, Decoupled effects of thermal cycle parameters on thermo-mechanical damage accumulation at fingers in crystalline silicon photovoltaic modules, Microelectron. Eng. 217 (2019) 111102, <https://doi.org/10.1016/j.mee.2019.111102>.
- [85] S. Roy, S. Kumar, R. Gupta, Investigation and analysis of finger breakages in commercial crystalline silicon photovoltaic modules under standard thermal cycling test, Eng. Fail. Anal. 101 (2019) 309–319, <https://doi.org/10.1016/j.engfailanal.2019.03.031>.
- [86] R. Meier, F. Kraemer, S. Wiese, K.-J. Wolter, J. Bagdahn, Thermal cycling induced load on copper-ribbons in crystalline photovoltaic modules, Reliab. Photovolt. Cells, Modul. Components, Syst. III 7773 (2010), <https://doi.org/10.1117/12.861350>, 777312-1.
- [87] J. Kasewieter, F. Haase, M.H. Larrodé, M. Köntges, Cracks in solar cell metallization leading to module power loss under mechanical loads, Energy Procedia 55 (2014) 469–477, <https://doi.org/10.1016/j.egypro.2014.08.011>.
- [88] A. Syed, Updated life prediction models for solder joints with removal of modeling assumptions and effect of constitutive equations, in: 7th Int Conf Therm Mech Multiphysics Simul Exp Micro-electronics Micro-systems, EuroSimE 2006, 2006, pp. 1–9, <https://doi.org/10.1109/ESIME.2006.1644010>, 2006.
- [89] K.B. Robert Darveaux, Constitutive relations for tin-based solder joints, IEEE Trans Components, Hybrid, Manuf Technol 15 (1992) 1013–1024.
- [90] H. Ma, Constitutive models of creep for lead-free solders, J. Mater. Sci. 44 (2009) 3841–3851, <https://doi.org/10.1007/s10853-009-3521-9>.
- [91] G. Cuddalorepatta, A. Dasgupta, Effect of primary creep behavior on fatigue damage accumulation rates in accelerated thermal cycling of Sn3.0Ag0.5Cu Pb-free interconnects, in: EuroSimE 2008 - Int Conf Therm Mech Multi-Physics Simul Exp Microelectronics Micro-systems, 2008, pp. 1–8, <https://doi.org/10.1109/ESIME.2008.4525095>.
- [92] G. Cuddalorepatta, A. Dasgupta, S. Sealing, J. Moyer, T. Tolliver, J. Loman, Durability of Pb-free solder between copper interconnect and silicon in photovoltaic cells, Prog. Photovoltaics Res. Appl. 18 (2010) 168–182, <https://doi.org/10.1002/pip.944>.
- [93] W.J.R. Song, S.K. Tippabhotla, A.A.O. Tay, A.S. Budiman, Effect of interconnect geometry on the evolution of stresses in a solar photovoltaic laminate during and after lamination, Sol. Energy Mater. Sol. Cells 187 (2018) 241–248, <https://doi.org/10.1016/j.solmat.2018.07.026>.
- [94] N. Bosco, T. Silverman, S. Kurtz, Simulation and experiment of thermal fatigue in the CPV die attach, AIP Conf Proc 1477 (2012) 267–271, <https://doi.org/10.1063/1.4753883>.
- [95] S. Kawai, T. Tanahashi, Y. Fukumoto, F. Tamai, A. Masuda, M. Kondo, Causes of degradation identified by the extended thermal cycling test on commercially available crystalline silicon photovoltaic modules, IEEE J Photovoltaics 7 (2017) 1511–1518, <https://doi.org/10.1109/JPHOTOV.2017.2741102>.
- [96] M.T. Zarmai, N.N. Ekere, C.F. Oduoza, E.H. Amalu, Optimization of thermo-mechanical reliability of solder joints in crystalline silicon solar cell assembly, Microelectron. Reliab. 59 (2016) 117–125, <https://doi.org/10.1016/j.microrel.2015.12.031>.
- [97] E.H. Amalu, D.J. Hughes, F. Nabhani, J. Winter, Thermo-mechanical deformation degradation of crystalline silicon photovoltaic (c-Si PV) module in operation, Eng. Fail. Anal. 84 (2018) 229–246, <https://doi.org/10.1016/j.engfailanal.2017.11.009>.
- [98] M. Owen-Bellini, J. Zhu, T.R. Betts, R. Gottschalg, Thermomechanical stresses of silicon photovoltaic modules, in: 13th Photovolt Sci Appl Technol Conf Bangor, UK, 2017.
- [99] J. Zhang, G. Li, X. Yuan, H. Zhao, Y. Yang, H. Li, et al., Relation of silver electrode solderability to intermetallic compound growth rate, J. Mater. Sci. Mater. Electron. 30 (2019) 7209–7215, <https://doi.org/10.1007/s10854-019-00972-3>.
- [100] K.J. Chen, F.Y. Hung, T.S. Lui, L.H. Chen, Y.W. Chen, Characterizations of Cu/Sn-Zn solder/Ag interfaces on photovoltaic ribbon for silicon solar cells, IEEE J Photovoltaics 5 (2015) 202–205, <https://doi.org/10.1109/JPHOTOV.2014.2373822>.
- [101] Y.J. Jeon, M.S. Kang, Y.E. Shin, Growth of an Ag3Sn intermetallic compound layer within photovoltaic module ribbon solder joints, Int J Precis Eng Manuf - Green Technol 7 (2020) 89–96, <https://doi.org/10.1007/s40684-019-00028-1>.
- [102] N. Jiang, A.G. Ebadi, K.H. Kishore, Q.A. Yousif, M. Salmani, Thermomechanical reliability assessment of solder joints in a photovoltaic module operated in a hot climate, IEEE Trans. Compon. Packag. Manuf. Technol. 10 (2020) 160–167, <https://doi.org/10.1109/TCMPT.2019.2933057>.
- [103] H. Nishikawa, N. Iwata, Formation and growth of intermetallic compound layers at the interface during laser soldering using Sn-Ag Cu solder on a Cu Pad, J. Mater. Process. Technol. 215 (2015) 6–11, <https://doi.org/10.1016/j.jmatprotec.2014.08.007>.
- [104] K.J. Chen, F.Y. Hung, T.S. Lui, L.H. Chen, Y.W. Chen, A study of green Sn-xZn photovoltaic ribbons for solar cell application, Sol. Energy Mater. Sol. Cells 143 (2015) 561–566, <https://doi.org/10.1016/j.solmat.2015.08.007>.
- [105] K.J. Chen, F.Y. Hung, T.S. Lui, L. Hsu, Low conductivity decay of Sn-0.7Cu-0.2Zn photovoltaic ribbons for solar cell application, Micromachines 10 (2019) 1–7, <https://doi.org/10.3390/mi10080550>.
- [106] K.J. Chen, F.Y. Hung, T.S. Lui, L. Hsu, Studies of interfacial microstructures and series resistance on electroplated and hot-dipped Sn-xCu photovoltaic modules, J. Electron. Mater. 47 (2018) 6028–6035, <https://doi.org/10.1007/s11664-018-6483-3>.
- [107] P. Schmitt, P. Kaiser, C. Savio, M. Tranitz, U. Eitner, Intermetallic phase growth and reliability of Sn-Ag-soldered solar cell joints, Energy Procedia 27 (2012) 664–669, <https://doi.org/10.1016/j.egypro.2012.07.126>.
- [108] C. Oh, A. Kim, J. Kim, J. Bang, J. Ha, W.S. Hong, Bonding copper ribbons on crystalline photovoltaic modules using various lead-free solders, J. Mater. Sci. Mater. Electron. 26 (2015) 9721–9726, <https://doi.org/10.1007/s10854-015-3640-9>.
- [109] T. Geipel, M. Moeller, J. Walter, A. Kraft, U. Eitner, Intermetallic compounds in solar cell interconnections: microstructure and growth kinetics, Sol. Energy Mater. Sol. Cells 159 (2017) 370–388, <https://doi.org/10.1016/j.solmat.2016.08.039>.
- [110] T. Geipel, M. Moeller, A. Kraft, U. Eitner, A comprehensive study of intermetallic compounds in solar cell interconnections and their growth kinetics, Energy Procedia 98 (2016) 86–97, <https://doi.org/10.1016/j.egypro.2016.10.084>.
- [111] S. Roy, S. Kumar, R. Gupta, Investigation and analysis of finger breakages in commercial crystalline silicon photovoltaic modules under standard thermal cycling test, Eng. Fail. Anal. (2019), <https://doi.org/10.1016/j.jengfailanal.2019.03.031>.
- [112] J. Jeong, N. Park, W. Hong, C. Han, Analysis for the degradation mechanism of photovoltaic ribbon wire under thermal cycling, in: Conf. Rec. IEEE Photovolt. Spec. Conf., IEEE, 2011, <https://doi.org/10.1109/PVSC.2011.6186611>, 003159–61.
- [113] O. Hasan, A.F.M. Arif, Performance and life prediction model for photovoltaic modules: effect of encapsulant constitutive behavior, Sol. Energy Mater. Sol. Cells 122 (2014) 75–87, <https://doi.org/10.1016/j.solmat.2013.11.016>.
- [114] W. Herrmann, N. Bogdanski, F. Reil, M. Köhl, K.-A. Weiss, M. Assmus, et al., PV module degradation caused by thermomechanical stress: real impacts of outdoor weathering versus accelerated testing in the laboratory, Reliab. Photovolt. Cells, Modul Components, Syst III 7773 (2010) 777301, <https://doi.org/10.1117/12.859809>.
- [115] Y. Aoki, M. Okamoto, A. Masuda, T. Doi, T. Tanahashi, Early failure detection of interconnection with rapid thermal cycling in photovoltaic modules, Jpn. J. Appl. Phys. 51 (2012) 10NF13, <https://doi.org/10.1143/JJAP.51.10NF13>.
- [116] A. Tummala, J. Oh, S. Tatapudi, G. Tamizhmani, Degradation of solder bonds in field aged PV modules: correlation with series resistance increase, in: 2017 IEEE 44th Photovolt Spec Conf PVSC 2017, 2017, <https://doi.org/10.1109/PVSC.2017.8366714>, 2912–7.
- [117] A. Sinha, O.S. Sastry, R. Gupta, Nondestructive characterization of encapsulant discoloration effects in crystalline-silicon PV modules, Sol. Energy Mater. Sol. Cells 155 (2016) 234–242, <https://doi.org/10.1016/j.solmat.2016.06.019>.
- [118] S. Chattopadhyay, R. Dubey, V. Kuthanazhi, J.J. John, C.S. Solanki, A. Kottantharayil, et al., Visual degradation in field-aged crystalline silicon PV modules in India and correlation with electrical degradation, IEEE J Photovoltaics 4 (2014) 1470–1476, <https://doi.org/10.1109/JPHOTOV.2014.2356717>.
- [119] C. Peike, S. Hoffmann, P. Hülsmann, B. Thaidigsmann, K.A. Weiß, M. Koehl, et al., Origin of damp-heat induced cell degradation, Sol. Energy Mater. Sol. Cells 116 (2013) 49–54, <https://doi.org/10.1016/j.solmat.2013.03.022>.
- [120] T.H. Kim, N.C. Park, D.H. Kim, The effect of moisture on the degradation mechanism of multi-crystalline silicon photovoltaic module, Microelectron. Reliab. 53 (2013) 1823–1827, <https://doi.org/10.1016/j.micrel.2013.07.047>.
- [121] R. Asadpour, X. Sun, M.A. Alam, Electrical signatures of corrosion and solder bond failure in c-Si solar cells and modules, IEEE J Photovoltaics 9 (2019) 759–767, <https://doi.org/10.1109/JPHOTOV.2019.2896898>.
- [122] R. Asadpour, R.V.K. Chavali, M.A. Alam, Physics-Based computational modeling of moisture ingress in solar modules: location-specific corrosion and delamination, in: Conf Rec IEEE Photovolt Spec Conf 2016, 2016, <https://doi.org/10.1109/PVSC.2016.7749725>, Novem:840–3.
- [123] N. Kim, C. Han, Experimental characterization and simulation of water vapor diffusion through various encapsulants used in PV modules, Sol. Energy Mater. Sol. Cells 116 (2013) 68–75, <https://doi.org/10.1016/j.solmat.2013.04.007>.
- [124] A. Kraft, L. Labusch, T. Ensslen, I. Durr, J. Bartsch, M. Glatthaar, et al., Investigation of acetic acid corrosion impact on printed solar cell contacts, IEEE J Photovoltaics 5 (2015) 736–743, <https://doi.org/10.1109/JPHOTOV.2015.2395146>.
- [125] T. Tanahashi, N. Sakamoto, H. Shibata, A. Masuda, Electrical detection of gap formation underneath finger electrodes on c-Si PV cells exposed to acetic acid vapor under hydrothermal conditions, in: Conf Rec IEEE Photovolt Spec Conf 2016, 2016, <https://doi.org/10.1109/PVSC.2016.7749778>, Novem:1075–9.
- [126] M.D. Kempe, G.J. Jorgensen, K.M. Terwilliger, T.J. McMahon, C.E. Kennedy, T. T. Borek, Acetic acid production and glass transition concerns with ethylene-vinyl acetate used in photovoltaic devices, Sol. Energy Mater. Sol. Cells 91 (2007) 315–329, <https://doi.org/10.1016/j.solmat.2006.10.009>.
- [127] A.W. Czanderna, F.J. Pern, Encapsulation of PV modules using ethylene vinyl acetate copolymer as a pottant: a critical review, Sol. Energy Mater. Sol. Cells 43 (1996) 101–181, [https://doi.org/10.1016/0927-0248\(95\)00150-6](https://doi.org/10.1016/0927-0248(95)00150-6).

- [128] A. Badiee, I.A. Ashcroft, R.D. Wildman, The thermo-mechanical degradation of ethylene vinyl acetate used as a solar panel adhesive and encapsulant, *Int. J. Adhesion Adhes.* 68 (2016) 212–218, <https://doi.org/10.1016/j.ijadhadh.2016.03.008>.
- [129] N. Kyranaki, J. Zhu, T.R. Betts, R. Gottschalg, The impact of acetic acid corrosion on the front-side contacts and the finger electrodes of c-Si PV cells. 14th photovolt., *Sci. Appl. Technol. Conf.* (2018) 1–5.
- [130] W. Gao, F. Huang, H. Tong, S. Yuan, G. Chen, Y. Yang, Effect of glass phase on solder joint reliability in crystalline silicon photovoltaic modules, *J. Mater. Sci. Mater. Electron.* 26 (2015) 7811–7814, <https://doi.org/10.1007/s10854-015-3429-x>.
- [131] J.-H. Kim, J. Park, D. Kim, N. Park, Study on mitigation method of solder corrosion for crystalline silicon photovoltaic modules, *Int. J. Photoenergy* 2014 (2014) 1–9, <https://doi.org/10.1155/2014/809075>.
- [132] Y. Ino, S. Asao, K. Shirasawa, H. Takato, Effect of soldering on the module degradation along bus bar in DH test and PCT for crystalline Si PV modules, in: 2018 IEEE 7th World Conf Photovoltaic Energy Conversion, WCPPEC 2018 - A Jt Conf 45th IEEE PVSC, 28th PVSEC 34th EU PVSEC, vol. 1, 2018, pp. 3552–3557, <https://doi.org/10.1109/PVSC.2018.8548219>.
- [133] B.H.B. Chudnovsky, W. Chester, Degradation of power contacts in industrial atmosphere: silver corrosion and whiskers, in: Proc Forty-Eighth IEEE Holm Conf Electr Contacts, 2002, pp. 140–150, <https://doi.org/10.1109/holm.2002.1040834>, 00.
- [134] A. Dolara, G.C. Lazaroiu, S. Leva, G. Manzolini, L. Votta, Snail trails and cell microcrack impact on PV module maximum power and energy production, *IEEE J Photovoltaics* 6 (2016) 1269–1277, <https://doi.org/10.1109/JPHOTOV.2016.2576682>.
- [135] S. Meyer, S. Timmel, M. Gläser, U. Braun, V. Wachtendorf, C. Hagendorf, Polymer foil additives trigger the formation of snail trails in photovoltaic modules, *Sol. Energy Mater. Sol. Cells* 55 (2014) 64–70, <https://doi.org/10.1016/j.solmat.2014.06.028>.
- [136] Jing Fan, Daliang Ju, Xiaoqin Yao, Zhen Pan, Mason Terry, William Gambogi, Katherine Stika, Junhui Liu, Wusong Tao, Zengsheng Liu, Yafeng Liu, Mai Wang, Qiuju Wu TJT, Study on snail trail formation in PV module through modeling and accelerated aging tests, *Sol. Energy Mater. Sol. Cells* 164 (2017) 80–86, <https://doi.org/10.1016/j.solmat.2017.02.013>.
- [137] H. Liu, C. Huang, W. Lee, S. Yan, F. Lin, A defect formation as snail trails in photovoltaic modules, *Energy Power Eng.* (2015) 348–353, <https://doi.org/10.4236/epe.2015.78032>, 07.
- [138] I. Duerr, J. Bierbaum, J. Metzger, J. Richter, D. Philipp, Silver grid finger corrosion on snail track affected PV modules - investigation on degradation products and mechanisms, *Energy Procedia* 98 (2016) 74–85, <https://doi.org/10.1016/j.egypro.2016.10.083>.
- [139] S. Meyer, S. Richter, S. Timmel, M. Gläser, M. Werner, S. Swatek, et al., Snail trails: root cause analysis and test procedures, *Energy Procedia* 38 (2013) 498–505, <https://doi.org/10.1016/j.egypro.2013.07.309>.
- [140] P. Peng, A. Hu, W. Zheng, P. Su, D. He, K.D. Oakes, et al., Microscopy study of snail trail phenomenon on photovoltaic modules, *RSC Adv.* 2 (2012) 11359–11365, <https://doi.org/10.1039/c2ra22280a>.
- [141] Y.H. Chou, W.Y. Chou, S.-M. Shiu, Y.C. Chien, S.Y. Huang, S. Chi, E. Wang RS, Chemical analysis and proposed generating mechanism for snail tracks contamination OF EVA encapsulated modules, in: Eur. Photovolt. Sol. Energy Conf. Exhib., 2011, pp. 3132–3136, <https://doi.org/10.1017/CBO9781107415324.004>.
- [142] N. Kim, K.J. Hwang, D. Kim, J.H. Lee, S. Jeong, D.H. Jeong, Analysis and reproduction of snail trails on silver grid lines in crystalline silicon photovoltaic modules, *Sol. Energy* 124 (2016) 153–162, <https://doi.org/10.1016/j.solener.2015.11.040>.
- [143] H. Yang, J. Chang, H. Wang, D. Song, Power degradation caused by snail trails in urban photovoltaic energy systems, *Energy Procedia* 88 (2016) 422–428, <https://doi.org/10.1016/j.egypro.2016.06.018>.
- [144] C.H. Huang, L De Chih, Y.C. Chen, M.Y. Huang, Z.C. Wu, S.J. Ho, Assessing the reliability and degradation of ribbon in photovoltaic module, in: Conf Rec IEEE Photovolt Spec Conf, vol. 2, 2011, <https://doi.org/10.1109/PVSC.2011.6186609>, 003150–2.
- [145] P. Hacke, M. Kempe, J.H. Wohlgemuth, L. Ji, Y.-C. Shen, Potential-induced degradation-delamination mode in crystalline silicon modules, in: 2016 Work Cryst. Silicon Sol. Cells Modul. Mater. Process., 2016, pp. 1–9.
- [146] J. Li, Y.C. Shen, P. Hacke, M. Kempe, Electrochemical mechanisms of leakage-current-enhanced delamination and corrosion in Si photovoltaic modules, *Sol. Energy Mater. Sol. Cells* 188 (2018) 273–279, <https://doi.org/10.1016/j.solmat.2018.09.010>.
- [147] H. Li, T. Yang, J. Huang, C. Chen, The neutral point shift of module string and delamination caused by potential-induced-degradation in 50 MWp photovoltaic power plant, in: 2018 IEEE 7th World Conf. Photovolt. Energy Conversion, WCPPEC 2018 - A Jt. Conf. 45th IEEE PVSC, 28th PVSEC 34th EU PVSEC, 2018, pp. 731–734, <https://doi.org/10.1109/PVSC.2018.8547898>.
- [148] V. Naumann, D. Lausch, A. Hänel, J. Bauer, O. Breitenstein, A. Graff, et al., Explanation of potential-induced degradation of the shunting type by Na decoration of stacking faults in Si solar cells, *Sol. Energy Mater. Sol. Cells* 120 (2014) 383–389, <https://doi.org/10.1016/j.solmat.2013.06.015>.
- [149] W. Luo, S. Khoo, P. Hacke, V. Naumann, D. Lausch, Potential-induced degradation in photovoltaic modules: a critical review, *Energy Environ. Sci.* 10 (2017) 43–68, <https://doi.org/10.1039/c6ee02271e>.
- [150] X. Yao, L. Herrera, S. Ji, K. Zou, J. Wang, Characteristic study and time-domain discrete-wavelet-transform based hybrid detection of series DC arc faults, *IEEE Trans. Power Electron.* 29 (2014) 3103–3115, <https://doi.org/10.1109/TPEL.2013.2273292>.
- [151] J. Flicker, J. Johnson, Electrical simulations of series and parallel PV arc-faults, *Conf. Rec. IEEE Photovolt. Spec. Conf.* (2013) 3165–3172, <https://doi.org/10.1109/PVSC.2013.6745127>.
- [152] F. Schimpf, L.E. Norum, Recognition of electric arcing in the DC-wiring of photovoltaic systems, in: INTELEC, Int. Telecommun. Energy Conf., IEEE, 2009, pp. 1–6, <https://doi.org/10.1109/INTLEC.2009.5352037>.
- [153] W.I. Bower, J.E. Granata, M.A. Quintana, S.S. Kuszmaul, J.E. Strauch, *Solar Module Arc Fault Modeling at Sandia National Laboratories*, 2010.
- [154] M.K. Alam, F. Khan, J. Johnson, J. Flicker, A comprehensive review of catastrophic faults in PV arrays: types, detection, and mitigation techniques, *IEEE J Photovoltaics* 5 (2015) 982–997, <https://doi.org/10.1109/JPHOTOV.2015.2397599>.
- [155] N.L. Georgijevic, M.V. Jankovic, S. Srdic, Z. Radakovic, The detection of series arc fault in photovoltaic systems based on the arc current entropy, *IEEE Trans. Power Electron.* 31 (2016) 5917–5930, <https://doi.org/10.1109/TPEL.2015.2489759>.
- [156] H. Chen, H. Zhao, D. Han, W. Liu, P. Chen, K. Liu, Structure-aware-based crack defect detection for multicrystalline solar cells, *Meas J Int Meas Confed* 151 (2020) 107170, <https://doi.org/10.1016/j.measurement.2019.107170>.
- [157] S. Kumar, P. Jena, A. Sinha, R. Gupta, Application of infrared thermography for non-destructive inspection of solar photovoltaic module, *J Non Destr Test Eval* (2017) 25–32.
- [158] A. Sinha, M. Bliss, X. Wu, S. Roy, R. Gottschalg, R. Gupta, Cross-characterization for imaging parasitic resistive losses in thin-film photovoltaic modules, *J Imaging* 2 (2016) 23, <https://doi.org/10.3390/jimaging2030023>.
- [159] R. Khatri, S. Agarwal, I. Saha, S.K. Singh, B. Kumar, Study on long term reliability of photo-voltaic modules and analysis of power degradation using accelerated aging tests and electroluminescence technique, *Energy Procedia* 8 (2011) 396–401, <https://doi.org/10.1016/j.egypro.2011.06.156>.
- [160] S. Kumar, R. Gupta, Investigation and analysis of thermo-mechanical degradation of fingers in a photovoltaic module under thermal cyclic stress conditions, *Sol. Energy* 174 (2018) 1044–1052, <https://doi.org/10.1016/j.solener.2018.10.009>.
- [161] M. Chicca, G. Tamizhmani, Nondestructive techniques to determine degradation modes: experimentation with 18 years old photovoltaic modules, in: 2015 IEEE 42nd Photovolt. Spec. Conf. PVSC 2015, IEEE, 2015, pp. 1–5, <https://doi.org/10.1109/PVSC.2015.7355709>.
- [162] T.L. Yang, K.Y. Huang, S. Yang, H.H. Hsieh, C.R. Kao, Growth kinetics of Ag3Sn in silicon solar cells with a sintered Ag metallization layer, *Sol. Energy Mater. Sol. Cells* 123 (2014) 139–143, <https://doi.org/10.1016/j.solmat.2014.01.018>.
- [163] H.T. Lee, M.H. Chen, Influence of intermetallic compounds on the adhesive strength of solder joints, *Mater. Sci. Eng., A* 333 (2002) 24–34, [https://doi.org/10.1016/S0921-5093\(01\)01820-2](https://doi.org/10.1016/S0921-5093(01)01820-2).
- [164] A.C.K. So, Y.C. Chan, J.K.L. Lai, Aging studies of Cu-Sn intermetallic compounds in annealed surface mount solder joints, *IEEE Trans. Compon. Packag. Manuf. Technol. Part B* 20 (1997) 161–166, <https://doi.org/10.1109/96.575568>.
- [165] H. Yang, W. He, H. Wang, J. Huang, J. Zhang, Assessing power degradation and reliability of crystalline silicon solar modules with snail trails, *Sol. Energy Mater. Sol. Cells* 187 (2018) 61–68, <https://doi.org/10.1016/j.solmat.2018.07.021>.
- [166] W. Oh, S. Kim, S. Bae, N. Park, S.-I. Chan, Y. Kang, et al., Migration of Sn and Pb from solder ribbon onto Ag fingers in field-aged silicon photovoltaic modules, *Int. J. Photoenergy* 2015 (2015) 1–7, <https://doi.org/10.1155/2015/257343>.
- [167] W. Luo, Y.S. Khoo, P. Hacke, V. Naumann, D. Lausch, S.P. Harvey, et al., Potential-induced degradation in photovoltaic modules: a critical review, *Energy Environ. Sci.* 10 (2017) 43–68, <https://doi.org/10.1039/c6ee02271e>.
- [168] A. Sinha, R. Gupta, Effects of different excitation waveforms on detection and characterisation of delamination in PV modules by active infrared thermography, *Nondestr. Test. Eval.* 32 (2017) 418–434, <https://doi.org/10.1080/10589759.2016.1265961>.